Efferocytes Release Extracellular Vesicles to Resolve Inflammation and Tissue Injury via Prosaposin-GPR37 Signaling

Purbasha Bhattacharya[1,2¶], Umesh Kumar Dhawan[3¶], Mohammed Tayab Hussain[3], Praveen Singh[1,2], Karran Kiran Bhagat[3], Aarushi Singhal[3], Shani Austin-Williams[3], Shantanu Sengupta[1,2], Manikandan Subramanian[2,3]

1, CSIR – Institute of Genomics and Integrative Biology, New Delhi, India

2, Academy of Scientific and Innovative Research (AcSIR), Ghaziabad 201002, India

3, William Harvey Research Institute, Faculty of Medicine and Dentistry, Queen Mary University of London, London, UK

¶ These authors contributed equally to this work

Lead contact:

Dr. Manikandan Subramanian
William Harvey Research Institute
Centre for Biochemical Pharmacology
Queen Mary University of London
Charterhouse Square
London EC1M6BQ
United Kingdom

Email: m.subramanian@qmul.ac.uk

Summary

Macrophages release soluble mediators following efferocytic clearance of apoptotic cells to facilitate intercellular communication and promote the resolution of inflammation. However, whether inflammation resolution is modulated by extracellular vesicles (EVs) and vesicular mediators released by efferocytes is not known. We report that efferocyte-derived EVs express prosaposin which binds to macrophage GPR37 to increase expression of the efferocytosis receptor Tim4 via an ERK-AP1 dependent signaling axis leading to increased macrophage efferocytosis efficiency and accelerated resolution of inflammation. Neutralization and knockdown of prosaposin or blocking GRP37 abrogates the pro-resolution effects of efferocyte-derived EVs *in vivo*. Administration of efferocyte-derived EVs in a murine model of atherosclerosis is associated with an increase in lesional macrophage efferocytosis efficiency and a decrease in plaque necrosis and lesional inflammation. Thus, we establish a critical role for efferocyte-derived vesicular mediators in increasing macrophage efferocytosis efficiency and accelerating the resolution of inflammation and tissue injury.

Introduction

Clearance of apoptotic cells (ACs) by macrophages (Mϕs) by a specialized process called efferocytosis plays a critical role in resolution of inflammation under various pathophysiological settings[1,2]. Crucially, impairment in the efferocytic process delays inflammation resolution and exacerbates pathology in multiple chronic inflammatory diseases such as chronic obstructive pulmonary disease (COPD), asthma, neurodegenerative diseases, and atherosclerosis[2]. For example, defective efferocytosis in advanced atherosclerosis is associated with plaque necrosis and thinning of the fibrous cap which results in plaque disruption, thrombosis, and myocardial infarction[3,4].

Understanding how Mϕ efferocytosis efficiency is regulated under physiological and pathological conditions is paramount for therapeutic targeting to ameliorate chronic inflammatory diseases associated with defective efferocytosis. Noteworthy, both efferocytosis and resolution of inflammation are critically regulated by intercellular communication[5]. For example, IL-13 released by regulatory T cells (Tregs) triggers IL-10 secretion by Mϕs which acts in an autocrine/paracrine manner to increase Mϕ efferocytosis efficiency[6]. Additionally, Mϕs that have engulfed ACs (efferocytes) secrete soluble mediators such as TGF-β, PGE2, IL-10, LXA4, and RvD1 as part of "post-engulfment" response to promote inflammation resolution[7-13]. Using *in vitro* and *in vivo* studies, several of these mediators have been shown to signal *in trans* to naïve Mϕs to enhance their efferocytosis efficiency[6,14-16]. In addition to soluble mediators, all cells release extracellular vesicles (EVs) containing proteins, mRNAs, and non-coding RNAs, which are then taken up by neighboring or distant cells to effect phenotypic change[17]. Most importantly, the cargo contained with the EVs may change in a dynamic fashion to reflect the cellular state of the host cell and thus directly regulate the outcome of intercellular communication during physiology and pathology[18-20]. In this context, the role of vesicular mediators released by efferocytes in further modulating Mϕ efferocytosis capacity and inflammation resolution is not known.

Herein, we show that efferocytes release EVs which increase the efferocytosis efficiency of naïve Mϕs in a feed-forward loop and skews them towards a pro-

reparative phenotype thereby promoting the resolution of inflammation *in vivo*. Mechanistically, we demonstrate that efferocytes release EVs that are enriched in prosaposin (PSAP) which triggers GPR37-mediated signaling on naïve Mϕs culminating in upregulation of Tim4, a key efferocytosis receptor[21]. Increased expression of Tim4 enhances Mϕ efferocytosis efficiency and ensures continuous AC uptake. These data establish a key role for efferocyte-derived vesicular mediators in intercellular communication with direct impact on the resolution of inflammation *in vivo*.

Results

Since efferocytosis leads to release of pro-resolving mediators[22], we asked whether efferocyte culture supernatants could enhance efferocytosis efficiency of naïve Mϕs. Indeed, treatment of naïve Mϕs with cell culture supernatants derived from efferocytes (Effero-CS) led to increased efferocytosis efficiency as compared with Mϕs that were incubated with culture supernatants derived from Ctrl Mϕs (**Figure 1A and Figure S1A**). Additionally, consistent with previous reports[12,13], treatment of Mϕs with Effero-CS suppressed the LPS-induced upregulation of *Nos2*, *Tnfa*, *Il1b* mRNA (**Figure S1B**) and the release of pro-inflammatory cytokine TNF (**Figure S1C**). Since all cells release extracellular vesicles (EVs) which play a critical role in intercellular communication in several physiological and pathophysiological settings, we questioned whether some of these effects could be mediated by EVs released by efferocytes. Towards this end, we subjected the culture supernatants to high-speed ultracentrifugation to obtain EV-depleted culture supernatant (**Figure S1D**). Interestingly, incubation of naïve Mϕs with Effero-CS that were depleted of EVs did not result in enhancement of efferocytosis efficiency (**Figure 1B**) suggesting a key role for EVs in increasing Mϕ efferocytosis. Next, we set out to directly test whether efferocyte-derived EVs affect efferocytosis efficiency of naïve Mϕs. EVs are classified according to size as microvesicles (0.2-1 μm) and small EVs (< 200 nm)[23]. Microvesicles (MVs) are derived by pinching from the plasma membrane while small EVs (EVs) are derived by budding from intracellular multivesiclular bodies[24]. Thus, MVs and EVs have distinct origins and could have biologically diverse functional effects. Hence, we subjected control and efferocyte-derived culture supernatants to differential ultracentrifugation and isolated fractions that are enriched in either MVs or EVs (**Figure S1E**). There was no significant difference in the concentration of EVs and MVs between the two groups (**Figure S1F**). When we incubated Mϕs individually with either Effero-EVs or Effero-MVs, we observed that Effero-EVs but not Effero-MVs were uniquely capable of recapitulating the efferocytosis enhancing capacity of Effero-CS (**Figure 1C**). Next, we tested whether Effero-EVs could suppress LPS-induced inflammatory mediator production by Mϕs. Indeed, Effero-EVs decreased the LPS-induced upregulation of *Nos2*, *Tnfa*, and *Il1b* mRNA expression (**Figure 1D**) suggesting that the anti-inflammatory effects of Effero-CS are in part mediated by EVs. Besides suppression of inflammation, treatment of

naïve Mϕs with Effero-EVs led to increased cell surface expression of CD206 (**Figure 1E**) and upregulation of genes such as *Arg1* and *Mrc1* indicating polarization of Mϕs towards a pro-reparative M2 phenotype (**Figure 1F**). Next, we characterized the EVs isolated from control Mϕs and efferocytes. Interestingly, the isolated EVs were ~120 nm in size (**Figure S1G**), displayed distinctive membrane morphology by cryo-EM[25] (**Figure S1H**), and expressed protein markers such as flotillin and CD9 (**Figure S1I**), features consistent with them being exosomes[23].
Since exosome biogenesis and release are regulated by neutral sphingomyelinase2 (nSMase2)[26], we asked whether inhibition of exosome release by efferocytes using GW4869, a nSMase2 inhibitor[27], could block the efferocytosis enhancing ability of Effero-CS. As expected, treatment of Mϕs with GW4869 led to a significant decrease in the number of EVs, but not MVs (**Figure S1J**). Importantly, the EV-deficient culture supernatant lost the ability to enhance efferocytosis efficiency of naïve Mϕs (**Figure 1G**). Note that GW4869 by itself does not affect efferocytosis (**Figure S1K**) excluding the possibility that carry-over of GW4869 in the culture supernatant directly inhibits Mϕ efferocytosis. Most importantly, a similar increase in efferocytosis efficiency was induced by Effero-EVs in human peripheral blood monocyte-derived Mϕs (**Figure 1H**). We next asked whether Effero-EVs affect continuous AC clearance since this is a critical determinant of inflammation resolution *in vivo*. Indeed, a higher proportion of Effero-EV-treated Mϕs were efficient at multiple AC uptake (**Figure 1I**).

Since efferocytes release pro-resolution molecules such as RvD1, LXA4, or IL-10, which are known to enhance Mϕ efferocytosis efficiency *in vitro*[6,10,14,16], we next tested whether the efferocytosis enhancing activity of Effero-EVs is mediated by passive surface adsorption of secreted pro-resolution molecules. However, this is not the case since Effero-EVs were able to enhance Mϕ efferocytosis efficiency in the presence of an IL-10 neutralising antibody (**Figure S1L**) and in *Alx/Fpr2*$^{-/-}$ (cognate receptor for RvD1 and LXA4) Mϕs (**Figure S1M**). Finally, AC-derived EVs were unable to increase Mϕ efferocytosis efficiency (**Figure S1N**) demonstrating that the efferocytosis-enhancing activity is specific to EVs released by Mϕs following the engulfment of ACs. In summary, these data suggest that Effero-EVs enhance naïve Mϕ efferocytosis efficiency, suppress production of pro-inflammatory cytokines, and promote polarization of Mϕs towards a pro-resolving M2 phenotype.

Effero-EVs promote inflammation resolution *in vivo*

Based on the *in vitro* data presented above, we next tested whether Effero-EVs increase Mϕ efferocytosis efficiency *in vivo*. Towards this goal, we injected Ctrl-EVs or Effero-EVs into the peritoneal cavity of mice followed by injection of fluorescently labelled ACs to test the efferocytosis efficiency of the resident peritoneal Mϕs. Consistent with our *in vitro* data, mice injected with Effero-EVs demonstrated a significant increase in Mϕ efferocytosis efficiency *in vivo* (**Figure 2A**).

Since the above experiments were conducted with *in vitro* generated Effero-EVs, we next questioned whether endogenously produced Effero-EVs affect Mϕ efferocytosis efficiency and inflammation resolution during pathophysiolological situations. We used zymosan-induced peritonitis as a murine model of acute self-resolving inflammation[28] to address this question. Zymosan elicits an acute and robust neutrophil infiltration into the peritoneal cavity which peaks at about 12 h post injection followed by local apoptosis and efferocytic clearance by Mϕs leading to spontaneous resolution of inflammation within 48 h[28]. To specifically test the role of EVs during the resolution phase of inflammation, we administered GW4869 (exosome biogenesis inhibitor) at 12 h post-zymosan injection and the mice were euthanized 12 h later. As expected, there was a significant reduction in the number of EVs in the peritoneal exudates of GW4869-treated mice (**Figure S2A**). Interestingly, the administration of GW4869 led to decreased Mϕ efferocytosis efficiency (**Figure 2B**) with concomitant increased accumulation of apoptotic neutrophils (**Figure 2C**). It is important to note that injection of GW4869 did not by itself impair Mϕ efferocytosis efficiency (**Figure S2B**). These data suggest that endogenously produced EVs can regulate Mϕ efferocytosis and, consequently, favor inflammation resolution. However, in this experimental set up, GW4869 blocks the release of EVs from all cell types and does not address the specific role of efferocyte-derived EVs in modulating inflammation resolution. To overcome this limitation, we next tested whether the impairment in Mϕ efferocytosis induced by GW4869 could be rescued by exogenous supplementation and selective replenishment of Effero-EVs into the peritoneal cavity. Towards this goal, we injected zymosan intraperitoneally and 12 h later the mice were randomized into three groups. One group received PBS (vehicle) while the other two groups were administered GW4869 along with either Ctrl-EVs or Effero-EVs. Peritoneal lavages

were analyzed at 18, 24, and 48 h post-zymosan injection to quantify myeloid cell infiltration, efferocytosis efficiency, and the kinetics of inflammation resolution (**Figure 2D**). First, we confirmed that the dose of EVs injected in these mice were within physiological range as demonstrated by the significantly lower numbers of EVs in GW4869-treated mice despite exogenous EV supplementation (**Figure S2C**). Interestingly, mice administered GW4869 showed increased neutrophil numbers in the peritoneal lavage as compared with vehicle-treated mice at all time points (**Figure 2E**). Since neither GW4869 nor EVs elicit neutrophil infiltration by itself (**Figure S2D and S2E**), these data suggest that the observed increase in neutrophil numbers could be due to an impairment in the inflammation resolution response upon abrogation of exosome release. In this context, we measured the time taken for neutrophil numbers to reach half-maximal, a parameter previously defined as the "resolution interval (Ri)" which is an indicator of the efficiency of inflammation resolution response. Consistent with our hypothesis, GW4869-treated mice showed a slower rate of decline in neutrophil numbers (**Figure 2E**) which was associated with an approximate doubling of the resolution interval, upto 36 h (**Figure 2F**). Interestingly, this impairment was significantly rescued in mice that received Effero-EVs with values ~20h, hence much closer to controls which had an Ri of 12h (**Figure 2F**). Most importantly, supplementation of Effero-EVs led to an increase in Mϕ efferocytosis efficiency (**Figure 2G and Figure S2F**) and more than halved the accumulation of apoptotic neutrophils within the exudate (**Figure 2H and Figure S2G**). Since Ctrl-EV treated mice had higher macrophage numbers as compared with Effero-EV-treated mice (Figure 2I), the decrease in accumulation of apoptotic neutrophils in the Effero-EV group (Figure 2H) is likely mediated by an increase in efferocytosis efficiency and not due to increased phagocyte availability.

EVs with pro-resolving activity are released by Mϕs specifically in response to ACs

As shown above, efferocytes release EVs that have pro-resolution activity *in vitro* and *in vivo*. Next, we asked whether these responses were specific to engulfment of ACs or a general phenomenon observed in response to engulfment of any biological material. To address this question, we isolated EVs from Mϕs engulfing distinct phagocytic targets such as ACs, necrotic cells, or IgG-coated ACs. All phagocytic targets were engulfed with similar efficiency (**Figure S3A**). Additionally, the number

of EVs released in the supernatant were equivalent among the groups (**Figure S3B**). The isolated EVs were incubated with naïve Mϕs for 16 h followed by analysis of efferocytosis efficiency. As expected, Effero-EVs increased Mϕ efferocytosis efficiency (**Figure 3A**). However, EVs isolated from Mϕs engulfing necrotic cells or IgG-coated live and IgG-coated ACs did not alter Mϕ efferocytosis efficiency (**Figure 3A**). Since all the phagocytic targets were derived from the same cell type, these data suggested that the release of EVs with pro-resolution activity is not dependent on signals derived from metabolism of the internalized biological material. Interestingly, these phagocytic targets are engulfed via distinct receptor-mediated mechanisms suggesting the involvement of specific proximal receptor-mediated signaling in triggering the pro-resolution response. Since Mertk and Axl play a critical role in recognition of ACs[29], we next tested whether these efferocytosis receptors are involved in signaling the downstream release of pro-resolving EVs. Consistent with this hypothesis, incubation of Mϕs with a Mertk or Axl activating antibody[11] led to release of EVs that enhances Mϕ efferocytosis efficiency (**Figure 3B**). In summary, these data suggest that pro-resolving EVs are released by Mϕs exposed to ACs following the activation of efferocytosis receptors Mertk and Axl.

Effero-EVs enhance the efficiency of AC binding

Since efferocytosis involves two key steps, namely, AC recognition via efferocytosis receptors and AC engulfment mediated by actin cytoskeletal reorganisation[30], we tested which of these steps are modulated by Effero-EVs. Towards this goal, Ctrl-EV and Effero-EV-exposed Mϕs were incubated with ACs in the presence of actin polymerization inhibitor cytochalasin D[31] which blocks AC engulfment[32] and allows the specific analysis of AC binding efficiency. Interestingly, the percentage of AC-bound Mϕs was significantly higher in the Effero-EV treated group (**Figure 3C**). In this context, we tested whether the enhanced AC binding is mediated by an increase in the levels of efferocytosis receptors. Flow-cytometric analysis demonstrated that Effero-EV-treated Mϕs had increased cell surface expression of the efferocytosis receptor Tim4 (**Figure 3D and E**) while others including Mertk, Axl, and LRP1 were unaffected (**Figure 3D**). The increase in Tim4 protein expression in Effero-EV-treated Mϕs was associated with increased *Timd4* mRNA expression (**Figure 3F**) suggesting a transcriptionally regulated response. Most importantly, the upregulation of Tim4 plays a causal role in this process because blocking Tim4 with a neutralizing

anti-Tim4 antibody[33] led to abrogation of the Effero-EV-induced increase in AC binding (**Figure 3G**). Overall, these data suggest that Effero-EVs increase AC binding by Mϕs via increased expression of the efferocytosis receptor Tim4.

Effero-EVs enhance Mϕ efferocytosis via PSAP-GPR37 signaling through ERK/AP-1 mediated transcriptional upregulation of Tim4

Since the numbers of EVs released by control and efferocytes were similar (**Figure S1F**), we speculated that the pro-resolving activity of Effero-EVs may be mediated by the specific cargo contained within them. In this regard, we conducted a SWATH MS-based proteomic analysis and identified the differentially expressed proteins between Ctrl- and Effero-EVs. Of the 1,055 total proteins identified, 89 proteins were significantly upregulated, and 82 proteins were downregulated in the Effero-EVs as compared with Ctrl-EVs (**Figure S4A**). We then manually curated the list of upregulated proteins to identify those with known or probable function in efferocytosis, phagocytosis, or inflammation, which led to a shortlist of 9 proteins (**Figure 4A**). We focused our attention on prosaposin (PSAP) which is the precursor protein for Saposins A-D and plays a key role in facilitating the lysosomal hydrolysis of sphingolipids[34]. Most importantly, PSAP can also be secreted and in its extracellular form is known to bind to GPR37[35], a G-protein coupled receptor that promotes Mϕ phagocytosis[36,37]. In this context, we speculated that EV-associated PSAP could play a role in increasing Mϕ efferocytosis efficiency and inflammation resolution responses. It is important to note that this mode of action for PSAP requires its presence on the surface of EVs to be able to interact with Mϕ GPR37. Indeed, PSAP immunostaining in non-permeabilized EVs followed by nano-flowcytometry (nano-FCM) confirmed that PSAP is present on the surface of EVs (**Figure 4B**) and that their expression is significantly increased in Effero-EVs (**Figure 4B**). Western blotting further confirmed that PSAP expression is increased in Effero-EVs (**Figure S4B**). Interestingly, we observed that Mϕs engulfing ACs demonstrate a modest increase in the intracellular level of PSAP (**Figure S4C**) which could potentially account for the increased expression on Effero-EVs.

Next, we tested whether EV-associated PSAP increases Mϕ efferocytosis efficiency. Towards this end, Mϕs were treated with Ctrl- or Effero-EVs in the presence of a neutralising anti-PSAP antibody. Interestingly, blocking PSAP completely blunted the ability of Effero-EVs to enhance efferocytosis efficiency (**Figure 4C**) suggesting a

key role for EV-associated PSAP in modulating Mϕ efferocytosis efficiency. To further confirm these findings, we knockdown PSAP in Mϕs by siRNA (**Figure S4D**) and then generated PSAP-deficient Effero-EVs (**Figure S4E**). PSAP-deficient Effero-EVs were unable to increase Mϕ efferocytosis efficiency (**Figure 4D**) or upregulate the expression of Tim4 (**Figure S4F**).

To test whether PSAP signals through Mϕ GPR37 to mediate its effects, we conducted efferocytosis assay in the presence of macitentan, a GPR37 and endothelin A/B receptor antagonist[38]. While macitentan by itself did not affect efferocytosis efficiency of naïve Mϕs (**Figure S4G**), its application to naïve Mϕs blocked the enhanced efferocytosis by Effero-EVs (**Figure 4E**). Most importantly, we confirmed that these effects were not due to the inhibition of endothelin A/B receptors because siRNA-mediated knockdown of GPR37 in Mϕs (**Figure S4H**) blocked the ability of Effero-EVs to increase the expression of Tim4 (**Figure S4I**) or increase efferocytosis efficiency (**Figure 4F**).

Since upregulation of Tim4 is crucial for Effero-EV-induced increase in Mϕ efferocytosis efficiency (**Figure 3G**), we sought to determine the signaling mechanism linking PSAP-mediated GPR37 activation to transcriptional upregulation of Tim4. Since GPR37 agonists are known to activate ERK signaling cascade[35,36], we specifically focused on AP-1 transcription factor which is known to be regulated by ERK[39] and is one of the top transcription factors binding to *Timd4* promoter[40]. First, we confirmed that Mϕs demonstrated rapid phosphorylation of ERK specifically in response to Effero-EVs (**Figure 5A**). Importantly, incubation of Mϕs with an ERK inhibitor blocked the ability of Effero-EVs to increase *Timd4* mRNA (**Figure 5B**) and Tim4 cell surface expression (**Figure 5C**). Interestingly, the expression of c-fos, a component of the AP-1 transcription factor complex, was increased in Mϕs incubated with Effero-EVs (**Figure 5D**). This increase was not due to direct transfer of c-fos from EVs since we could not detect c-fos expression in EVs isolated from both Ctrl as well as Effero-EVs (**Figure S5A**). Furthermore, the increase in c-fos can be blocked by inhibiting ERK activation (**Figure 5D**) suggesting an ERK-mediated regulation of c-fos expression. Finally, consistent with our hypothesis, SR 11302, an AP-1 inhibitor[41], blocked the Effero-EV-induced increase in expression of *Timd4* mRNA (**Figure 5E**) and Tim4 cell surface expression (**Figure 5F**), and abrogated the efferocytosis promoting activity of Effero-EVs (**Figure 5G**). Overall, these data

suggest a key role for the PSAP-GPR37-ERK-AP1 signaling axis in regulating the expression of Tim4 and Mϕ efferocytosis efficiency.

Effero-EVs promote Mϕ efferocytosis *in vivo* through prosaposin-GPR37 signaling

Next, we set out to test the *in vivo* relevance of EV-associated PSAP in regulating Mϕ efferocytosis. PSAP plays a dichotomous role in inflammation and Mϕ polarization depending on its cellular localization, for example, intracellular PSAP polarizes Mϕs towards a pro-inflammatory M1 phenotype[42] while our data demonstrates that extracellular PSAP skews Mϕs towards a pro-resolving M2 phenotype. Therefore, we resorted to a neutralizing antibody approach to specifically block the function of extracellular EV-associated PSAP while preserving the function of intracellular PSAP. To test whether EV-associated PSAP is mechanistically linked to enhancement of Mϕ efferocytosis and resolution of tissue injury *in vivo*, we turned to a mouse model of dexamethasone-induced thymocyte apoptosis. The administration of dexamethasone leads to extensive synchronous thymocyte apoptosis followed by thymic Mϕ-mediated efferocytosis which leads to thymus shrinkage, loss of tissue cellularity, and resolution of tissue injury[43,44]. In this model, one group of mice were administered an anti-PSAP neutralizing antibody to specifically block the action of extracellular EV-associated PSAP while another group received appropriate IgG as control. Eighteen hours after dexamethasone injection, thymic cellularity, thymocyte apoptosis, and in situ efferocytosis efficiency were quantified. Compared with the vehicle and IgG-treated group, mice that received anti-PSAP Ab showed a significant increase in thymic cellularity (**Figure S5B**) and accumulation of apoptotic thymocytes (**Figure 6A**) suggestive of defective efferocytosis. To directly test this possibility, we next conducted an in-situ efferocytosis assay[45] in which we quantified the numbers of TUNEL+ apoptotic thymocytes that are either free or associated with a Mac2+ Mϕ. The mice administered dexamethasone along with either vehicle or IgG had comparable efferocytosis efficiency (**Figure 6B**). In contrast, the administration of anti-PSAP Ab led to a significant decrease in the ratio of Mϕ-associated TUNEL+ ACs to free ACs (**Figure 6B**). Since the numbers of thymic Mϕs was similar between the groups (**Figure S5C**), these data suggest that blocking the endogenously produced

extracellular EV-associated PSAP leads to a decrease in macrophage efferocytosis efficiency and inflammation resolution *in vivo*. Finally, we observed a significant decrease in expression of Tim4 on thymic Mϕs in mice administered PSAP nAb (**Figure 6C and Figure S5D**).

To complement these findings, we tested whether the increase in Mϕ efferocytosis upon exogenous administration of Effero-EVs is dependent on the presence of PSAP. To test this hypothesis, mice injected with dexamethasone were randomized into four groups each receiving either vehicle, Ctrl-EVs, Effero-EVs isolated from negative control siRNA transfected Mϕs, or Effero-EVs isolated from PSAP siRNA knockdown Mϕs (**Figure S4E**). Mice injected with Effero-EVs showed a significant decrease in thymic cellularity (**Figure S5E**) and had lower numbers of annexin-V+ ACs (**Figure 6D and Figure S5F**) as compared with mice injected either vehicle or Ctrl-EVs. Most importantly, these effects were absent in mice that were administered Effero-EVs isolated from PSAP-knockdown efferocytes (**Figure 6D and Figure S5F**). Interestingly, mice injected with Effero-EVs demonstrated a higher ratio of Mϕ-associated TUNEL+ ACs to free ACs (**Figure 6E**). Since there was no difference in Mϕ numbers between the groups (**Figure S5G**), these data indicate that Effero-EVs enhanced Mϕ efferocytosis efficiency. Most importantly, this increase in efferocytosis efficiency was blunted in mice injected with PSAP-deficient Effero-EVs (**Figure 6E**). Finally, we confirmed increased expression of Tim4 on thymic Mϕs in mice administered Effero-EVs which was absent in mice that received PSAP-deficient Effero-EVs (**Figure 6F**). These data together suggests that EV-associated PSAP increases Mϕ efferocytosis efficiency via upregulation of Tim4.

Next, using the dexamethasone thymocyte apoptosis model system described above, we tested whether the ability of PSAP-enriched Effero-EVs to enhance Mϕ efferocytosis efficiency is mediated via GPR37 signaling. Towards this end, dexamethasone injected mice were randomized into four groups receiving either Ctrl EVs or Effero-EVs without or with the GPR37 antagonist macitentan. As above, compared with Ctrl-EVs, mice administered Effero-EVs demonstrated lower thymocyte count (**Figure S5H**), decreased numbers of ACs (**Figure 6G and Figure S5I**), and increased *in situ* Mϕ efferocytosis efficiency (**Figure 6H**), all of which were abrogated upon treatment with macitentan (**Figure 6G and H**). In mice receiving Ctrl-EVs, the administration of macitentan did not affect thymocyte count, the

numbers of ACs, or thymic Mϕs (**Figure 6G, and Figure S5H-J**). However, there was a modest decrease in Mϕ efferocytosis efficiency (**Figure 6H**) which is consistent with the pro-resolving role of GPR37 described previously[36]. Overall, in conjunction with the *in vitro* studies, these *in vivo* data show that the efferocytosis enhancing activity of Effero-EVs is dependent upon PSAP-GPR37 signaling.

Effero-EVs enhance lesional Mϕ efferocytosis efficiency and resolve inflammation in advanced atherosclerotic plaques

Impairment in the efferocytic process and the consequent failure to resolve inflammation leads to adverse pathological and clinical outcomes in atherosclerosis[2,3]. Therefore, strategies that enhance Mϕ efferocytosis efficiency could represent high value therapeutic approaches[4]. In this context, we tested whether therapeutic administration of Effero-EVs can reverse the impairment in lesional Mϕ efferocytosis efficiency and promote inflammation resolution in a murine model of atherosclerosis. Since our *in vitro* and *in vivo* findings show that Effero-EVs increase Mϕ efferocytosis efficiency via GPR37 signaling, we first tested whether atherosclerotic plaque Mϕs express GPR37. Immunostaining analysis confirmed that Mac2+ Mϕs in atherosclerotic plaques of *Apoe*$^{-/-}$ mice express GPR37 (**Figure 7A**) raising the possibility that these Mϕs could be amenable to functional modulation by Effero-EVs. To test the effect of Effero-EVs on atherosclerosis progression, we fed atherosclerosis-prone *Apoe*$^{-/-}$ mice with a high fat high cholesterol western type-diet for eight weeks followed by randomization of the animals into three groups. Then, one group received PBS (vehicle) while the other two groups received either Ctrl-EVs or Effero-EVs via intraperitoneal injections three times a week over the following 6 weeks (**Figure 6B**). Body weight, blood glucose, plasma cholesterol, plasma triglyceride, and leukocyte numbers were similar between the three groups of mice measured at the end of experiment (**Figure S6A-E**). Next, using biotinylated-EVs, we confirmed that the injected EVs entered the atherosclerotic plaques (**Figure S6F**). Interestingly, their localization largely overlapped with lesional Mac2+ Mϕs (**Figure S6F**). To test whether the plaque-migrated Effero-EVs could increase lesional Mϕ efferocytosis efficiency, we next conducted an *in situ* efferocytosis assay. Like our *in vitro* and *in vivo* data with peritoneal Mϕs and thymic Mϕs presented above, analysis of aortic root atherosclerotic plaques demonstrated that the number of TUNEL+ ACs that colocalized with Mac2+ Mϕs was significantly

higher in the Effero-EV group compared with vehicle and Ctrl-EV groups indicating an improvement in lesional Mϕ efferocytosis efficiency (**Figure 7C**). Consistent with the enhanced efferocytosis, the Effero-EV group demonstrated significant reduction in lesion area and plaque necrosis (**Figure 7D-G**). Additionally, the Effero-EV group had higher intimal collagen content (**Figure 7H**). We next conducted plaque cellular phenotyping and observed that the Effero-EV group had a relatively higher proportion of smooth muscle cells (**Figure 7I**) and lower numbers of Mϕs (**Figure 7J**) as compared with the Ctrl-EV group. Also, vascular inflammation was significantly attenuated in the Effero-EV group as indicated by decreased expression levels of pro-inflammatory genes (**Figure S6G**) and increased expression of markers of alternatively activated M2 Mϕs (**Figure S6H**). Additionally, consistent with the anti-inflammatory effects, the Effero-EV group showed decrease levels of TNF in the plasma while IL1β was unchanged. Finally, the Effero-EV group demonstrated increased expression of Tim4 in lesional Mϕs (**Figure 7K**), a molecular signature of PSAP-GPR37 signaling-mediated enhancement of efferocytosis. These data demonstrate that administration of Effero-EVs increased the expression of Tim4 on plaque Mϕs and led to higher lesional Mϕ efferocytosis efficiency likely via PSAP-GPR37 signaling, which was associated with decreased plaque necrosis, suppression of vascular inflammation and enhanced M2 Mϕ polarization, increased smooth muscle cell numbers and collagen deposition, suggesting an overall remodeling of the atherosclerotic plaque towards a stable phenotype.

Discussion

Extensive intercellular communication is a prerequisite for successful resolution of inflammation following tissue injury[5]. The clearance of ACs by Mϕs and the subsequent post-engulfment response involving the release of several soluble factors including cytokines, growth factors, and specialized pro-resolving mediators plays an integral role in promoting cellular crosstalk[2,4]. In this study, we extend these findings further, and establish EVs released by efferocytes as key mediators of intercellular communication by playing a critical role in i) enhancing Mϕ efferocytosis efficiency in a feed-forward loop, ii) promoting the polarization of Mϕs towards a pro-reparative M2 phenotype, and iii) promoting resolution of inflammation under pathological settings such as in atherosclerosis. Mechanistically, we show that efferocytes release PSAP+ EVs which acts via GPR37 on naïve Mϕs to enhance their efferocytic capacity. This process involves PSAP-GPR37-mediated activation of ERK signaling which increases the expression of c-fos (AP-1 transcription complex) resulting in the transcriptional upregulation of Tim4, a key Mϕ efferocytosis receptor, leading to enhanced AC recognition and continuous clearance.

At sites of inflammation, the number of ACs far outpace the number of available phagocytes[1]. Therefore, mechanisms that enhance the efferocytosis efficiency of Mϕs or those that increase their capacity to continuously engulf ACs are crucial for rapid clearance of dead cells and restoration of tissue homeostasis. In this context, we and others have previously described mechanisms that enhance the ability of Mϕs to continuously clear ACs, for example, UCP2-mediated lowering of mitochondrial membrane potential[43]; SLC2A1-mediated enhanced glycolysis leading to Rac1 activation[46]; DRP1-mediated mitochondrial fragmentation promoting focal exocytosis of endomembranes to developing phagosome[32]; AC-derived arginine that activates Dbl/Rac1 pathway to promote multiple AC uptake[44]; and epigenetic repression mediated by AC-derived methionine[45]. Recently, efferocytosis-induced proliferation of Mϕs was proposed as a mechanism for increasing phagocyte pool at sites of inflammation and promote rapid clearance of dying cells[47]. It is important to note that all these efferocytosis-enhancing mechanisms act *in cis* and are cell-autonomous requiring Mϕs to initially ingest an AC which then triggers signaling cascades that make them better at engulfing the subsequently encountered ACs. In

this context, our data advances several concepts. First, we describe a mechanism by which vesicular mediators released by efferocytes signal *in trans* to enhance efferocytosis efficiency of naïve bystander Mϕs and skew them towards a pro-reparative M2 phenotype. Secondly, we show that the release of EVs with pro-resolution properties are not dependent on ingestion and degradation of ACs but triggered by proximal ligation of efferocytosis receptors such as Mertk and Axl. This is particularly intriguing and raises the possibility that Mϕs encountering ACs, but not necessarily clearing them, may also be involved in inflammation resolution via generation and release of pro-resolving EVs which increase Tim4 expression on resident and infiltrating Mϕs.

Tim4 can directly bind phosphatidylserine exposed on ACs and acts as a tethering receptor[48]. However, the short cytoplasmic tail of Tim4 lacks intracellular signaling motifs and therefore is dependent on co-receptors such as BAI1, Mertk, and integrins to promote rearrangement of actin cytoskeletal with the ensuing engulfment of AC[49,50]. In inflammatory microenvironment, efferocytosis receptors such as Mertk undergo ectodomain cleavage mediated by sheddases like ADAM17 and this results in a decreased density of AC recognition receptors on Mϕs[11,51]. Since Tim4 can associate with several membrane receptors to signal AC engulfment, we speculate that the Effero EV-induced increased expression of Tim4 could serve as a compensatory mechanism to preserve efferocytosis efficiency in inflammatory environments.

Mϕ-derived EVs have been shown to have pro-inflammatory or anti-inflammatory activity depending on the site and polarization state of the Mϕs. For example, Mϕs cultured under hyperglycemia-mimicking condition release EVs that increase bone marrow hematopoeisis and myeloid cell infiltration in atherosclerotic plaques[52]. Similarly, ox-LDL-treated THP1 cell-derived EVs worsen atherosclerosis via enhanced ROS generation and NETosis[53]. In contrast, *in vitro* M2 Mϕ-derived EVs suppress production of inflammatory cytokines *in vitro* and administration of these EVs to western diet fed *Apoe*$^{-/-}$ mice led to decreased numbers of peripheral blood neutrophils and monocytes and was associated with decreased atherosclerotic plaque necrosis[54]. Interestingly, the administration of Effero EVs in our study did not alter peripheral blood monocyte or neutrophil numbers. In a recent study, MSC-

derived exosomes were shown to express MFGE8 which serves as an opsonin for ACs and promotes their clearance leading to attenuation of myocardial ischemic injury[55]. Similarly, cardiosphere-derived EVs enhanced cardioprotection in a mouse model of myocardial ischemia-reperfusion injury via enhanced Mertk-mediated Mϕ efferocytosis[56]. These studies taken together with our findings highlight that EVs from several cellular sources can act in concert to promote Mϕ efferocytosis via distinct molecular mechanisms.

Prosaposin (PSAP) is a precursor protein for saposins which facilitates lysosomal hydrolysis of sphingolipids[57]. Consequently, mutations and loss of activity of saposins leads to lysosomal storage disorders[57]. In addition to its intracellular function, full-length prosaposin can be secreted to exert neuroprotective functions via action on neuronal GPR37[34]. Our data demonstrates that extracellular PSAP can also be secreted anchored on, or embedded in, EVs to exert its actions. It is of interest that recent studies have shown that tissue resident Mϕs express GPR37 and respond to multiple agonists such as prosaposin, prosaptide (TX14), neuroprotectin D1 (NPD1), and the anti-malarial drug artesunate to promote Mϕ phagocytic activity, resolve inflammatory pain, and provide protection from infection-induced sepsis[36,37]. While these studies addressed the role of Mϕ GPR37 and its agonism using a pharmacological approach, our demonstration that endogenous Effero EVs are enriched in PSAP provides a physiological context wherein this pathway could be operative to resolve inflammation.

Recently, lipid-loaded Mϕs such as atherosclerotic plaque Mϕs were shown to have increased intracellular expression of PSAP which was associated with altered cellular metabolism leading to increased glycolysis and pro-inflammatory polarization[42]. Furthermore, loss of Mϕ PSAP expression in *Ldlr*$^{-/-}$ mice led to decreased atherosclerotic lesion area and reduced plaque inflammation highlighting the pro-inflammatory and pro-atherogenic role of cellular PSAP[42]. In contrast to these effects of intracellular PSAP, our data demonstrates that extracellular PSAP, for instance when associated with EVs, signals via GPR37 to promote Mϕ efferocytosis efficiency and polarization of Mϕs towards a pro-reparative phenotype. In *Apoe*$^{-/-}$ mice, Effero-EVs decreased atherosclerotic plaque necrosis, lowered lesional inflammation, and increased collagen deposition. Overall, these data

highlight the dichotomous role of PSAP on Mϕ function which is dependent on intracellular *vs.* extracellular localization and the activation of specific signaling cascades.

The administration of EVs, particularly exosomes from various cellular sources including Mϕs and mesenchymal stem cells, have been used extensively as a therapeutic strategy to promote tissue repair following injury in several preclinical animal models of disease[58]. Indeed, cellular engineered EVs are in clinical trials for the treatment of cancer, infectious diseases, and stroke[59]. Their use presents certain challenges particularly the batch-to-batch variability which is a significant concern in its use as therapy[59]. In this context, the identification of PSAP as a specific mediator of the beneficial efferocytosis enhancing and pro-resolving effects of Effero EVs acting via GPR37 signaling, may enable the future development of targeted therapeutic strategies focused on GPR37 agonists such as artesunate or prosaptides like TX-14, PS18, and retro-inverso D5. Furthermore, the mechanistic insight from our study enables the development of nanomedicine approaches to enhance Mϕ efferocytosis efficiency and promote inflammation resolution and tissue repair in a tissue and cell-targeted manner.

In summary, our study establishes the release of pro-resolving vesicular mediators by efferocytes as a critical arm of the AC post-engulfment response during physiology. Additionally, our data supports the exploitation of PSAP-GPR37 signaling axis as an interesting strategy to enhance efferocytosis efficiency of Mϕs and its ability to continuously clear ACs in the settings of dysregulated inflammation resolution such as in atherosclerosis and other chronic inflammatory diseases.

Limitations of the study

To examine the physiological role of endogenous EVs in inflammation resolution, we used GW4869 to block the release of exosomes. Like all chemical inhibitors, GW4869 could have off-target effects and on-target effects that could affect inflammation and its resolution. To mitigate confounding effects, we examined whether functional phenotypes could be reversed by replenishing EVs by exogenous administration. Additionally, although we suggest a role for AC-mediated Mertk and Axl signaling in triggering the release of pro-resolving EVs, it is important to note that

other efferocytosis receptors could possibly mediate a similar effect. Finally, we show that PSAP is enriched in Effero-EVs but how signaling via the efferocytosis receptors mediate the sorting of PSAP into EVs remains to be tested in future studies.

Acknowledgements

This work was supported by funding to MS from DBT-Wellcome Trust India Alliance Fellowship (IA/I/17/2/503295) and Barts Charity (MGU0459). P.B. was supported by CSIR Senior Research Fellowship. U.D. and A.S. are funded by QMUL Principal studentship. The authors thank CSIR-Institute of Genomics and Integrative Biology for infrastructure support and acknowledge funding from Barts Charity grant MGU0509 for supporting nano-flowcytometry.

Author contributions

P.B., U.D., and M.S. designed and conducted experiments, analyzed data, and wrote the manuscript. M.T.H., A.S., P.S., K.K.B, S.A.W., and S.S.G. conducted experiments, analyzed data, and edited the manuscript.

Declaration of interests

The authors declare no competing interests.

Figure legends

Figure 1. Efferocyte-derived EVs increase efferocytosis efficiency of naive Mϕs. **(A)** Efferocytosis assay in BMDMs treated for 16 h with Ctrl- or Effero-CS. **(B)** Similar to **(A)**, except that the appropriate groups of CS were subjected to high-speed ultracentrifugation to deplete EVs. **(C)** Efferocytosis assay in BMDMs treated with MVs or EVs obtained from Ctrl- or Effero-CS. **(D)** qPCR-based analysis of gene expression in BMDMs incubated with vehicle, Ctrl-, or Effero-EVs for 16 h followed by exposure to LPS (10 ng/mL) for 6 h. (**E)** Flow-cytometry for the quantification of cell surface expression levels of CD206 in BMDMs exposed to Ctrl- or Effero-EVs. **(F)** Similar to E, except that the treated cells were subjected to qPCR-based analysis of gene expression of *Arg1* and *Mrc1*. **(G)** Efferocytosis assay in BMDMs exposed to CS obtained from Ctrl

Mϕs, efferocytes, or efferocytes pre-treated with GW4869 (5 μM). **(H)** Quantification of efferocytosis efficiency in human PB-MDMs treated with Ctrl- or Effero-EVs. **(I)** Continuous efferocytosis assay by sequential incubation with pHrodo-red and pHrodo-green-labelled ACs in BMDMs treated with Ctrl- or Effero-EVs. Bar, 10 μm. The dots in the scatter plot represent the number of independent biological replicates.

Figure 2. Efferocyte-derived EVs promote inflammation resolution *in vivo*. (A) *In vivo* efferocytosis assay in mice 16 h after administration of Ctrl- or Effero-EVs intraperitoneally (equivalent to 30 μg of EV protein). **(B and C)** 10-week-old female C57BL/6 mice were injected 1 mg zymosan intraperitoneally and 12 h later were randomized to receive either PBS (vehicle) or GW4869 (2.5 mg/kg, ip). Mice were euthanized 24 h post-injection of zymosan and the peritoneal lavage was analyzed for **(B)** Mϕ efferocytosis efficiency as the percentage of F4/80+ Mϕs that co-stain for neutrophil marker Ly6G intracellularly and **(C)** the number of Annexin-V positive apoptotic neutrophils. n = 3 mice per group. **(D)** Schematic of the experimental strategy. **(E)** Flow-cytometric analysis of the numbers of neutrophils in the peritoneal lavage at indicated time points in appropriate groups of mice. **(F)** The bar graph represents Resolution Interval (Ri) which was defined as the time taken for neutrophil numbers to reach half-maximal. Ri was calculated as shown by the dotted lines in E. **(G)** Efferocytosis efficiency of peritoneal Mϕs in the indicated groups of mice was calculated as the percent F4/80+ cells that stain positive for intracellular Ly6G. **(H)** Percentage of Annexin-V+ neutrophils in the peritoneal lavage. **(I)** Mϕ numbers in the peritoneal lavage of the indicated groups of mice at various time points. n = 3 mice per group.

Figure 3. Effero-EVs enhance AC recognition via upregulation of efferocytosis receptor Tim4. (A) Efferocytosis assay was conducted in BMDMs incubated with EVs isolated from Mϕs that have engulfed either ACs (Effero EVs), necrotic cells (NC), IgG-opsonized ACs (IgG AC), or IgG-coated live cells (IgG Live). **(B)** Similar to (A), except that EVs were isolated from Mϕs exposed to ACs (Effero EVs) or activating antibodies against Axl or Mertk. **(C)** AC binding assay in indicated groups of Mϕs. **(D and E)** Analysis of the expression levels of Tim4, Mertk, Axl, and LRP1 on Mϕs exposed to vehicle or EVs as indicated. **(F)** qPCR-based analysis of expression of Tim4 mRNA expression in Ctrl- and Effero-EV-treated Mϕs **(G)** Efferocytosis assay was conducted in

BMDMs exposed to control or Effero-EVs followed by incubation with fluorescently labelled ACs in the presence of a Tim4 neutralizing antibody, anti-Mac2 antibody, or isotype antibody control. The dots in the bar graph represent data points from individual biological replicates.

Figure 4. EV-associated PSAP increases Mϕ efferocytosis efficiency via GPR37 signaling. (A) The heatmap shows the shortlist of manually curated proteins with known functions in phagocytosis and/or inflammation that are significantly upregulated in the Effero-EVs as compared with Ctrl-EVs. **(B)** Analysis of surface levels of PSAP on Ctrl- and Effero-EVs by nano-flowcytometry. **(C)** Efferocytosis assay in BMDMs incubated with PBS (vehicle), Ctrl,- or Effero-EVs in the presence of neutralizing anti-PSAP antibody. **(D)** Efferocytosis assay in BMDMs incubated with Ctrl- or Effero-EVs derived from Mϕs transfected with negative control siRNA (siNC) or PSAP siRNA (siPSAP). **(E)** Efferocytosis assay in BMDMs exposed to PBS (vehicle), Ctrl-, or Effero-EVs in the absence or presence of macitentan (10 nM). **(F)** Efferocytosis assay in Control (siNC Mϕ) and GPR37 knockdown (siGPR37 Mϕ) BMDMs exposed to Ctrl- or Effero-EVs.

Figure 5. Effero-EVs upregulate Tim4 expression via a GPR37/ERK/AP-1 signaling axis. (A) Immunoblotting for phospho-ERK (pERK) and total ERK (tERK) in whole cell lysates of BMDMs exposed to vehicle, Ctrl-, or Effero-EVs for 20 min. **(B and C)** BMDMs were treated with vehicle, Ctrl-, or Effero-EVs in the absence or presence of PD980459 (ERK inh, 10 μM) followed by analysis of **(B)** *Timd4* mRNA expression by qPCR or **(C)** cell surface expression levels of Tim4 by flow-cytometry. **(D)** c-fos immunobolot in whole cell lysates of BMDMs treated with either vehicle, Ctrl-, or Effero-EVs. **(E – G)** BMDMs were treated with vehicle, Ctrl-, or Effero EVs in the absence or presence of SR11302 (AP-1 inh, 10 μM) followed by analysis of **(E)** *Timd4* gene expression by qPCR, **(F)** Tim4 cell surface expression by flow cytometry, and **(G)** efferocytosis efficiency.

Figure 6. Effero-EVs enhance Mϕ efferocytosis efficiency *in vivo* via PSAP-GPR37 signaling. (A-C) 8-week-old female C57BL/6 mice were injected dexamethasone along with either PBS (Veh), anti-PSAP neutralizing Ab (50 μg), or control IgG. 18 h post-

injection, the following parameters were analyzed in the thymus: **(A)** The numbers of annexin-V positive ACs, **(B)** in-situ efferocytosis efficiency of thymic Mϕs on sections of thymus immunostained with anti-Mac2 antibody to detect Mϕs (green) and TUNEL labeling to detect ACs (red). Efferocytosis efficiency (right panel) was calculated as the ratio of ACs that are associated with a Mϕ (white arrows) vs. those that are lying free (white arrowheads). Bar, 25 μm. **(C)** Cell surface expression levels of Tim4 on F4/80+ thymic Mϕs. n=5 mice per group. **(D-F)** 8-week-old female mice were injected dexamethasone intraperitoneally followed by intravenous administration of Ctrl- or Effero-EVs isolated from either PSAP knockdown (siPSAP) or Ctrls (siNC) followed by analysis of **(D)** annexin-V+ cells by flow-cytometry, **(E)** in-situ thymic Mϕ efferocytosis efficiency, and **(F)** analysis of Tim4 expression on thymic Mϕs. **(G-H)** As above, except that appropriate groups of mice were administered dexamethasone without or with macitentan (Maci, 10 mg/kg ip). n=5 mice per group.

Figure 7. Effero-EVs enhance lesional Mϕ efferocytosis efficiency and decrease plaque necrosis in advanced atherosclerosis. (A) Aortic root sections were immunostained with anti-Mac2 (green) and anti-GPR37 (red) antibodies. Nuclei were stained with DAPI (blue). Bar, 100 μm. **(B)** Schematic showing the experimental strategy for evaluating the effect of Effero-EVs on atherosclerosis progression in *Apoe*$^{-/-}$ mice. **(C)** In-situ efferocytosis assay in aortic root sections of indicated groups of mice was conducted by staining with TUNEL reagent (green) and anti-Mac2 antibody (red). The white arrows indicate TUNEL+ ACs that are associated with Mac2+ Mϕs while the white arrowheads show free-lying TUNEL+ cells. Lesional Mϕ efferocytosis efficiency was calculated as the ratio of Mϕ-associated ACs: free ACs (right panel). Bar, 25 μm. **(D)** Representative H&E-stained aortic root sections of indicated groups of mice which were used for quantification of total lesion area **(E)**, total necrotic area **(F)**, and % necrotic area **(G)**. The black dashed lines in (D) demarcate areas of plaque necrosis. **(H)** Representative images of trichrome-stained aortic root sections of indicated groups of mice and quantification of lesional collagen content. Bar, 50 μm. **(I and J)** The bar graph shows quantified data of lesional smooth muscle cell (SMC) and Mϕ content in indicated groups of mice immunostained with anti-sm-actin and anti-Mac2 antibody respectively. **(K)** Representative images of aortic root sections immunostained with anti-Mac2 (green) and anti-Tim4 (red) antibody respectively. The integrated fluorescence intensity of Tim4

on Mac2+ regions of the plaque was quantified (bar graph, right panel). Bar, 50 μm. **(L)** qPCR-based analysis of the expression levels of *Timd4* mRNA in atherosclerotic carotid arteries of indicated groups of mice. n = 10 mice per group.

STAR★Methods

Resource availability

Lead contact

Resource and reagents requests should be directed to the lead contact, Dr. Manikandan Subramanian (m.subramanian@qmul.ac.uk)

Materials availability

The study did not generate new unique reagents.

Data and code availability

- All data reported in this paper will be shared by the lead contact upon request.
- This paper does not report original code.
- Any additional information required to reanalyze the data reported in this paper is available from the lead contact upon request.

Experimental models and subject details

Animals and maintenance

C57BL/6 and *Apoe*$^{-/-}$ (Stock # 002052) mice were purchased from Charles River and Jackson laboratories, respectively, and were maintained in the Biological Service Unit (BSU) of Queen Mary University of London, UK. A separate cohort of C57BL/6 mice were bred and maintained at CSIR-Institute of Genomics and Integrative Biology, New Delhi. All mice were maintained in IVC cages with 12 h light-dark cycle and had access to ad libitum food and water. Sex matched male and female C57BL/6 mice aged on average between 8-12 weeks, without any previous procedure history were used in the experiments. For the induction of atherosclerosis, *Apoe*$^{-/-}$ mice were fed high-fat high-cholesterol western type diet (SDS western diet, 829100) for 14 weeks. *Alx/Fpr2*$^{-/-}$ mice were a kind gift from Prof. Mauro Perretti, Queen Mary University of London. All mice were randomly assigned to experimental procedures. The investigators were blinded to treatment groups for atherosclerosis, dexamethasone-induced thymocyte apoptosis, and *in vivo* peritoneal cavity efferocytosis assays. All animal procedures were conducted in accordance with

ethical guidelines after obtaining approval from the Home Office, UK, and the Institutional Animal Ethics Committee of CSIR-Institute of Genomics and Integrative Biology, New Delhi.

Cell lines and cell culture

Human leukemia monocytic cell line, THP-1, mouse Mϕ like cells RAW 264.7 cells, L-929 mouse fibroblasts, and human immortalized T lymphocyte cell line Jurkat were obtained from ATCC and cultured in RPMI supplemented with 10% (vol/vol) heat inactivated fetal bovine serum (GIBCO) and penicillin-streptomycin in an incubator at 37°C. THP-1 cells were differentiated into Mϕs by treatment with 100 ng/ml PMA (Sigma-Aldrich) for 24 hours followed by culturing in fresh media for another 48 hours. None of these cell lines have been listed in the database of cross-contaminated or misidentified lines.

Primary mouse BMDM culture

Bone marrow cells were obtained by flushing the marrow of 8–10-week-old female or male *C57BL/6* mice as described previously[61]. The cells were cultured in DMEM supplemented with 10% (vol/vol) FBS and 20% (vol/vol) L-929 cell culture supernatant. On day 3, half the medium was replaced with fresh Mϕ culture medium. Fully differentiated Mϕs were harvested on day 7 for further experiments.

Human monocyte derived macrophages

30 ml peripheral blood was collected by venipuncture from healthy adult donors after obtaining informed consent. All the human participants were aged between 25-30 years and comprised of both sexes. The protocol was approved by the Institutional Human Ethics Committee of CSIR-Institute of Genomics and Integrative Biology, New Delhi. PBMCs were isolated by Ficoll-Hypaque density gradient centrifugation following manufacturer's protocol. The isolated PBMCs were cultured for 7 days in DMEM supplemented with 10% human AB serum and 50 ng/ml M-CSF.

Methods details

AC generation

THP1 monocytic cells, Jurkat cells, or mouse splenocytes were rendered fluorescent by labelling with either PKH67, PKH26, or CellVue Claret according to

manufacturer's (Sigma) protocol. For selected experiments (indicated in figure legend), cells were labelled with the pH-sensitive dye pHrodo-red (Thermofisher, 20 ng/ml) or pHrodo-green (20 ng/ml) in PBS (pH 8.5) for 30 min followed by 2 washes in complete medium. For induction of apoptosis, fluorescently labelled cells were exposed to UV-C (254 nm) for 5 min (3.6 kJ/m^2) followed by incubation for 1 h at 37°C. We routinely obtain > 90% Annexin-V+ ACs using this protocol.

***In vitro* efferocytosis assay**

BMDMs or differentiated THP-1 Mϕs were plated at a density of 0.5x10^6 cells/well in a 24-well plate. Fluorescently labelled ACs were incubated with Mϕs at a 3:1 AC:Mϕ ratio for 1 h followed by 3 washes with PBS to remove unbound ACs. Fluorescence microscopy imaging was conducted on an EVOS FL microscope. Image analysis was conducted using Fiji (ImageJ). Efferocytosis efficiency was calculated as the percentage of total Mϕs that contains at least one fluorescently labeled AC.

***In vitro* continuous AC clearance assay**

Mϕs plated at a density of 0.5x10^6 cells/well in 24 well-plate were incubated with pHrodo red-labelled ACs at a ratio of 3:1 (AC:Mϕ) for 45 min followed by 3 washes with PBS to remove unbound ACs. A second round of pHrodo green-labelled AC at a ratio of 3:1 was added and incubated for 1 h. 3 rinses with PBS was conducted to remove unengulfed cells. Imaging was conducted on EVOS FL fluorescence microscope. The proportion of pHrodo-red+ Mϕs that are also positive for pHrodo-green signal were used for calculation of the efficiency of multiple AC uptake.

AC binding assay

Mϕs were treated with cytochalasin D (1 μM) for 30 min prior to addition of fluorescently labelled ACs at a Mϕ:AC ratio of 1:3. After 1 h, the unbound ACs were removed by 3 washes with cold PBS followed by fluorescence microscopy to quantify the percent Mϕs that have bound an AC.

EV isolation and their *in vitro* and *in vivo* utilization

For experiments involving isolation of EVs, Mϕs were cultured in DMEM supplemented with 10% exosome-depleted FBS (Thermofisher). For EV isolation, culture supernatants were subjected to differential ultracentrifugation as described

previously[62]. Briefly, the supernatant was centrifuged at 300x*g* for 10 min at 4°C to remove cells followed by another spin at 2000 x*g* at 4°C for 10 min to remove dead cells and debris. Subsequently, the supernatant was centrifuged at 10,000 x*g* for 30 min at 4°C to remove microvesicles. Finally, the supernatant was transferred to polycarbonate ultracentrifuge tubes and centrifuged at 100,000 x*g* for 70 minutes at 4°C in Type 70 Ti rotor of Beckman Coulter ultracentrifuge. The EV pellet was washed once by resuspending in PBS followed by another round of centrifugation at 100,000 x*g* at 4°C for 70 minutes. The final EV pellet was resuspended in 1X PBS and NTA was conducted to determine EV concentration. For *in vitro* experiments, Mϕs were incubated with EVs for 16 h at a Mϕ:EV ratio of 1:100. For *in vivo* experiments, EVs were lysed with RIPA buffer and protein concentration was estimated using BCA assay and mice were injected 30 µg protein equivalent of EVs intravenously per mouse.

Nanoparticle tracking analysis (NTA)

To check for the size distributions and concentration of EVs, Nanoparticle Tracking Analysis (NTA) was used (NanoSight NS300, Malvern instruments, UK). The NanoSight NS300 with a 488 nm laser was used to detect the vesicles. Sample from each group was diluted to 1:1000 dilution with 1X PBS and was applied to the instrument through 1 ml syringe. The data was analysed at 25 frames per second and measurements were made every 60 s at 25°C. The particles size distribution and concentration in particles/mL were determined using the properties of light scattering and Brownian motion. The raw data were exported to Graphpad Prism for data visualization.

NanoFCM

Fluorescently labelled EVs were quantified by high resolution flow cytometry using a Flow NanoAnalyzer Instrument (NanoFCM, Inc.). The NanoAnalyzer was calibrated using dual-laser quality control beads (NanoFCM, Inc.) and Silica Nanospheres Cocktail #1 (65-155nm; NanoFCM, Inc.) to standardise particle concentration and size, respectively. An aliquot of the preferential solvent for EV samples was acquired as a blank control. Quality control beads, sizing beads and fluorescently labelled EVs were all acquired on the NanoAnalyzer with a sampling pressure of 1.0kPa and events recorded for a total of 1 minute.

Cryo-EM

To prepare samples for cryo-EM study, lacey carbon grids (Cu, 300 mesh) were glow-discharged (45s at MED RF power level) in Harrick plasma cleaner. 4 µL of sample solution was applied on to the carbon side of EM grid, which was then blotted for 2.5 s at 95% humidity and plunge-frozen into Leica GP2 plunger (Queen Mary University of London). Grids were imaged on a Jeol JEM-2100 plus (Queen Mary University of London), equipped with Gatan OneView 16MP camera at accelerating voltage of 200 kV. Images were obtained using SerialEM software at low dose mode at 50k magnification, corresponding to 2.166Å with the defocus range set from -2.5 to -5 µm.

RNA isolation, cDNA, and qPCR

Total RNA was isolated from cells using RNeasy Mini Kit (QIAGEN, Valencia, CA, and USA) according to the manufacturer's protocol. 1 µg of total RNA was converted into cDNA using PrimeScript™ 1st strand cDNA Synthesis Kit (TaKaRa). To analyse gene expression, synthesized cDNA was mixed with KAPA SYBR Green master mix as a fluorescent reporter and gene-specific primers pairs which are listed in **Table S1**. 18s RNA was used as a housekeeping gene. qRT-PCR was conducted using Roche Lightcycler 480. Relative gene expression was calculated using the ΔΔCt method and the expression was normalized to reference gene. All measurements were carried out in technical triplicates and appropriate numbers of biological replicates as indicated in the figure legend.

Western blotting

Whole cell lysates were generated by lysis in 2X Laemmli buffer. EVs were lysed using RIPA buffer (Merck) and the protein concentration was measured using BCA protein assay (ThermoFisher). The lysates were further mixed with 5X-Laemmli buffer. 25 µg of protein/well was loaded on to 10% SDS-PAGE gel. After electrophoresis, the resolved proteins were transferred to PVDF membrane (Millipore, USA). The membranes were blocked with 5% BSA or 5% non-fat milk for 1 h followed by incubation with antibodies against flotillin-1, CD-9, Calnexin, PSAP, pERK, tERK, or c-fos for 16 h at 4°C with constant gentle shaking. After 3 washes with TBST, the membranes were incubated with respective HRP-conjugated

secondary antibodies (1:5000) and chemiluminescent signal was captured on an Azure 400 Imager (Azure biosystems). The images were exported as a TIFF file and densitometric analysis was conducted using ImageJ. The details of all antibodies used in this study are presented in **Key Resource Table**.

Flow cytometry

Cells were suspended in PBS containing 3% FBS at a density of 10^7 cells/ml and incubated on ice for 30 min with Fc blocker (anti-mouse CD16/CD32). Cell surface staining was conducted by incubation with fluorophore conjugated antibodies for 1 h on ice. Cells were washed twice with PBS and then analyzed on a BD LSRFortessa. For detection of apoptosis, cells were resuspended in annexin V-binding buffer and incubated with annexin V-FITC for 15 min at room temperature. Data were analyzed using FlowJo (Version 10).

Zymosan-induced peritonitis

Acute self-resolving sterile peritonitis was induced in 10-week-old female C57BL/6 mice by injection of zymosan A (1 mg/mouse) intraperitoneally. Peritoneal exudate was collected at indicated time points and the cells were pelleted by centrifugation at 300 x*g* for 10 min. The supernatant was stored at -80°C for future analysis. The cells were stained with annexin-V FITC and fluorophore-conjugated anti-F4/80 and anti-Ly6G for assessment of total numbers of ACs, neutrophils, and Mϕs respectively by flow cytometry. For assessment of *in situ* efferocytosis, cells labelled with anti-F4/80 antibody were permeabilized and incubated with anti-Ly6G antibody and flow cytometry was conducted. Efferocytosis efficiency was quantified as the percent F4/80+ cells that co-stain with Ly6G. Non-permeabilized cells labelled with anti-F4/80 and Ly6G served as control.

***In vivo* peritoneal cavity efferocytosis assay**

$1x10^6$ PKH67 or CellVue Claret-labelled ACs suspended in a volume of 300 µl of PBS were injected intraperitoneally. 1 h post-injection, the mice were euthanized, and peritoneal lavage was conducted. The lavage fluid was centrifuged, and the cell pellet was stained with anti-F4/80 antibody for 30 min on ice. After 2 washes with PBS, efferocytosis efficiency was quantified as the percent F4/80+ cells that co-stain with PKH67 using flow cytometry.

Mass spectrometry

Proteomic analysis for Ctrl EVs and Effero EVs were performed using data independent acquisition-based SWATH-MS (sequential window acquisition of all theoretical mass spectra) method. EVs were lysed in 100 µl of RIPA buffer, centrifuged at 15000 *xg* for 10 mins at 4°C and supernatant was collected in fresh 1.5 ml microcentrifuge tubes. TCA-acetone method was used for protein precipitation and pellets were resuspended in Tris-HCl (100 mM) with 8 M urea, pH 8.5. Protein quantitation was done using Bradford assay. 20 µg of protein from each sample was reduced with 25 mM of Dithiothreitol (DTT) for 30 mins at 56°C, followed by alkylation using 55 mM of Iodoacetamide (IAA) at room temperature (in dark) for 30 mins. These samples were then subjected to trypsin digestion in an enzyme to substrate ratio of 1:10 (trypsin: protein) for 16 hours at 37°C.The tryptic peptides were vacuum dried in a vacuum concentrator.

Peptides from each sample were cleaned up using a C18 Ziptip (Merck, USA) as per manufacturer's protocol. SWATH-MS analysis for the samples was performed on a quadrupole-TOF hybrid mass spectrometer (TripleTOF 6600, SCIEX) coupled to an Eksigent NanoLC-425 system. Optimized source parameters were used, curtain gas and nebulizer gas were maintained at 25 psi and 30 psi respectively, the ion spray voltage was set to 5.5 kV at a temperature of 250°C. Peptides were loaded on a trap-column (ChromXP C18CL 5 µm 120 Å, Eksigent, SCIEX) and online desalting was performed for 10 mins, at a flow rate of 10 µl/min. Peptides were separated on a reverse-phase C18 analytical column (ChromXP C18, 3 µm 120 Å, Eksigent, SCIEX) in a 57 min long gradient with a flow rate of 5 µl/min using water with 0.1% formic acid and acetonitrile with 0.1% formic acid.

SWATH method was created with 96 precursor isolation windows, defined based on precursor m/z frequencies in DDA run using the SWATH Variable Window Calculator (SCIEX), with a minimum window of 5 m/z. Data was acquired using Analyst TF 1.7.1 Software (SCIEX). Accumulation time was set to 250 msec for the MS scan (400–1250 m/z) and 25 msec for the MS/MS scans (100–1500 m/z). Rolling collision energies were applied on +2 charged ions for each window based on the m/z range of each SWATH, with a collision energy spread of 5 eV. Total cycle time was 3.1 sec.

SWATH-MS Data analysis: The SWATH-MS raw files with .wiff extension were analyzed in Spectronaut 15 software from Biognosys using directDIA workflow. A *Homo sapiens* protein database from UniprotKB with 20,396 entries (Swiss-Prot) was used and protein identification was performed with 1% FDR. directDIA analysis was performed with default settings; cross-run data normalization was performed where normalization strategy was set to automatic. Quantitative data was exported in the form of 'Run Pivot Report' and differential protein analysis was performed in Microsoft Excel.

siRNA transfection

Transfection was performed using RNAimax reagent (ThermoFisher) according to the manufacturer's prescribed protocol. Briefly, cells were seeded in 24 well plates for *in vitro* cell-based assays and in a petri dish for isolating EVs for *in vivo* use. Lipofectamine® RNAiMAX reagent was diluted in Opti-MEM® Medium (Gibco) and mixed with 10 nmol siRNA targeting PSAP (Invitrogen, Cat # 4390772) or GPR37 (Qiagen, Cat # 5104411918) diluted in an equal volume of Opti-MEM® Medium and incubated for 5 min at room temperature to allow formation of siRNA-lipofectamine complexes. Cells were incubated with the siRNA complex in Opti-MEM for 12 h followed by replacement with DMEM supplemented with 10% (vol/vol) heat-inactivated FBS 10 U/mL penicillin, and 100 mg/mL streptomycin. 24 h after transfection, cells were used for further experiments or validation of knockdown.

***In vivo* thymic efferocytosis assay**

8-week-old female C57BL/6 mice were injected 250 µg of dexamethasone (in 250 µl PBS) intraperitoneally. 18 h later, the mice were euthanized, and thymus was harvested. One lobe of the thymus was dissected and fixed in formalin followed by paraffin embedding and sectioning. Thymus sections were stained with anti-Mac2 antibody and TUNEL to quantify *in situ* efferocytosis efficiency as the ratio of TUNEL+ cells that are associated with Mac2+ Mϕs vs. those that are free. The other thymic lobe was disaggregated and total thymocyte numbers were counted. The cells were then stained with fluorophore-conjugated annexin-V and anti-F4/80 antibody to quantify the numbers of ACs and F4/80+ Mϕs by flow cytometry.

Atherosclerotic plaque morphometry and lesional *in situ* efferocytosis assay

After euthanasia, mice were perfused with PBS via intracardiac injection. The heart along with aortic root was dissected and fixed in 10% neutral buffered formalin followed by embedding in paraffin blocks. 8 µm thick serial sections were cut starting from the first appearance of the tricuspid valve. For analysis of total lesion area and necrotic area, H&E staining was conducted on 6 equally spaced sections encompassing the entire aortic root. For immunofluorescence assays, the aortic root sections were subjected to antigen retrieval using citrate buffer (10 mM sodium citrate, 0.05% tween-20, pH 6.0) as described previously[63]. The sections were then blocked with 3% FBS (in PBS) followed by incubation with appropriate primary antibody (details in table below) at 4°C for 16 h. After 3 washes with PBS, the sections were incubated with appropriate fluorophore-conjugated secondary antibody for 1 h at room temperature. Images were captured using a fluorescence microscope (EVOS FL2, ThermoFisher) and the data were anlayzed using Fiji (ImageJ). *In situ* efferocytosis assay was conducted as described previously. Briefly, TUNEL staining was performed following manufacturer's instructions (ThermoFisher). Following TUNEL labeling, the sections were immunostained with anti-Mac2 antibody and counterstained with DAPI. Fluorescence microscopy was performed and the *in situ* efferocytosis efficiency was calculated as the ratio of TUNEL+ ACs that are associated with a Mac2+ Mϕ (associated) or lying free (Associated:Free).

Biotinylation of EVs

EVs were incubated with EZ-link sulfo-NHS-biotin (5 mM, Thermofisher) in PBS pH8.5 for 30 min at 37°C. The excess and unbound biotin was removed by ultrafiltration using a 10 kDa MWCO filter (Millipore).

Metabolic parameters and CBC

Blood glucose was measured in 5 h fasted mice using commercially available glucose test strips and glucometer (Accu-Chek). Commercially available kits were used for measurement of plasma total cholesterol (CH200, Randox) and triglyceride (TR 210, Randox) following manufacturer's protocol. CBC analysis was conducted on an automated IDEXX Procyte Dx haematology analyzer.

Quantification and Statistical analysis

All data are presented as mean±SEM unless indicated otherwise. For statistical analysis, all data were tested for normal distribution using Shapiro-Wilk test. Data that followed normal distribution were subjected to parametric test such as Student's t-test for comparison of two groups or one-way ANOVA followed by Sidak's multiple comparisons test was conducted for detecting statistical difference between more than two groups.

Table S1. List of primers used for qPCR-based analysis of gene expression.

References

1. Morioka, S., Maueröder, C., and Ravichandran, K.S. (2019). Living on the Edge: Efferocytosis at the Interface of Homeostasis and Pathology. Immunity *50*, 1149-1162. https://doi.org/10.1016/j.immuni.2019.04.018.

2. Doran, A.C., Yurdagul, A., and Tabas, I. (2020). Efferocytosis in health and disease. Nature Reviews Immunology *20*, 254-267. 10.1038/s41577-019-0240-6.

3. Kojima, Y., Weissman, I.L., and Leeper, N.J. (2017). The Role of Efferocytosis in Atherosclerosis. Circulation *135*, 476-489. 10.1161/circulationaha.116.025684.

4. Dhawan, U.K., Singhal, A., and Subramanian, M. (2021). Dead cell and debris clearance in the atherosclerotic plaque: Mechanisms and therapeutic opportunities to promote inflammation resolution. Pharmacological Research *170*, 105699. https://doi.org/10.1016/j.phrs.2021.105699.

5. Serhan, C.N., Gupta, S.K., Perretti, M., Godson, C., Brennan, E., Li, Y., Soehnlein, O., Shimizu, T., Werz, O., Chiurchiù, V., et al. (2020). The Atlas of Inflammation Resolution (AIR). Molecular Aspects of Medicine *74*, 100894. https://doi.org/10.1016/j.mam.2020.100894.

6. Proto, J.D., Doran, A.C., Gusarova, G., Yurdagul, A., Jr., Sozen, E., Subramanian, M., Islam, M.N., Rymond, C.C., Du, J., Hook, J., et al. (2018). Regulatory T Cells Promote Macrophage Efferocytosis during Inflammation Resolution. Immunity *49*, 666-677.e666. 10.1016/j.immuni.2018.07.015.

7. Fadok, V.A., Bratton, D.L., Konowal, A., Freed, P.W., Westcott, J.Y., and Henson, P.M. (1998). Macrophages that have ingested apoptotic cells in vitro inhibit proinflammatory cytokine production through autocrine/paracrine mechanisms involving TGF-beta, PGE2, and PAF. J Clin Invest *101*, 890-898. 10.1172/jci1112.

8. Voll, R.E., Herrmann, M., Roth, E.A., Stach, C., Kalden, J.R., and Girkontaite, I. (1997). Immunosuppressive effects of apoptotic cells. Nature *390*, 350-351. 10.1038/37022.

9. Zhang, S., Weinberg, S., DeBerge, M., Gainullina, A., Schipma, M., Kinchen, J.M., Ben-Sahra, I., Gius, D.R., Yvan-Charvet, L., Chandel, N.S., et al. (2019). Efferocytosis Fuels Requirements of Fatty Acid Oxidation and the Electron Transport Chain to Polarize Macrophages for Tissue Repair. Cell Metab *29*, 443-456.e445. 10.1016/j.cmet.2018.12.004.

10. Dalli, J., and Serhan, C.N. (2012). Specific lipid mediator signatures of human phagocytes: microparticles stimulate macrophage efferocytosis and pro-resolving mediators. Blood *120*, e60-72. 10.1182/blood-2012-04-423525.

11. Cai, B., Thorp, E.B., Doran, A.C., Subramanian, M., Sansbury, B.E., Lin, C.S., Spite, M., Fredman, G., and Tabas, I. (2016). MerTK cleavage limits proresolving mediator biosynthesis and exacerbates tissue inflammation. Proc Natl Acad Sci U S A *113*, 6526-6531. 10.1073/pnas.1524292113.

12. Bonnefoy, F., Gauthier, T., Vallion, R., Martin-Rodriguez, O., Missey, A., Daoui, A., Valmary-Degano, S., Saas, P., Couturier, M., and Perruche, S. (2018). Factors Produced by Macrophages Eliminating Apoptotic Cells Demonstrate Pro-Resolutive Properties and Terminate Ongoing Inflammation. Front Immunol *9*, 2586. 10.3389/fimmu.2018.02586.

13. Martin-Rodriguez, O., Gauthier, T., Bonnefoy, F., Couturier, M., Daoui, A., Chagué, C., Valmary-Degano, S., Gay, C., Saas, P., and Perruche, S. (2021). Pro-Resolving Factors Released by Macrophages After Efferocytosis Promote Mucosal Wound Healing in Inflammatory Bowel Disease. Front Immunol *12*, 754475. 10.3389/fimmu.2021.754475.

14. Godson, C., Mitchell, S., Harvey, K., Petasis, N.A., Hogg, N., and Brady, H.R. (2000). Cutting edge: lipoxins rapidly stimulate nonphlogistic phagocytosis of apoptotic neutrophils by monocyte-derived macrophages. J Immunol *164*, 1663-1667. 10.4049/jimmunol.164.4.1663.

15. Dalli, J., and Serhan, C.N. (2019). Identification and structure elucidation of the pro-resolving mediators provides novel leads for resolution pharmacology. Br J Pharmacol *176*, 1024-1037. 10.1111/bph.14336.

16. Frasch, S.C., Fernandez-Boyanapalli, R.F., Berry, K.Z., Leslie, C.C., Bonventre, J.V., Murphy, R.C., Henson, P.M., and Bratton, D.L. (2011). Signaling via macrophage G2A enhances efferocytosis of dying neutrophils by augmentation of Rac activity. J Biol Chem *286*, 12108-12122. 10.1074/jbc.M110.181800.

17. van Niel, G., D'Angelo, G., and Raposo, G. (2018). Shedding light on the cell biology of extracellular vesicles. Nature Reviews Molecular Cell Biology *19*, 213-228. 10.1038/nrm.2017.125.

18. Sherman, C.D., Lodha, S., and Sahoo, S. (2021). EV Cargo Sorting in Therapeutic Development for Cardiovascular Disease. Cells *10*. 10.3390/cells10061500.

19. Oggero, S., Austin-Williams, S., and Norling, L.V. (2019). The Contrasting Role of Extracellular Vesicles in Vascular Inflammation and Tissue Repair. Front Pharmacol *10*, 1479. 10.3389/fphar.2019.01479.

20. Yates, A.G., Pink, R.C., Erdbrügger, U., Siljander, P.R.-M., Dellar, E.R., Pantazi, P., Akbar, N., Cooke, W.R., Vatish, M., Dias-Neto, E., et al. (2022). In sickness and in health: The functional role of extracellular vesicles in physiology and pathology in vivo. Journal of Extracellular Vesicles *11*, e12190. https://doi.org/10.1002/jev2.12190.

21. Miyanishi, M., Tada, K., Koike, M., Uchiyama, Y., Kitamura, T., and Nagata, S. (2007). Identification of Tim4 as a phosphatidylserine receptor. Nature *450*, 435-439. 10.1038/nature06307.

22. Saas, P., Vetter, M., Maraux, M., Bonnefoy, F., and Perruche, S. (2022). Resolution therapy: Harnessing efferocytic macrophages to trigger the resolution of inflammation. Front Immunol *13*, 1021413. 10.3389/fimmu.2022.1021413.

23. Théry, C., Witwer, K.W., Aikawa, E., Alcaraz, M.J., Anderson, J.D., Andriantsitohaina, R., Antoniou, A., Arab, T., Archer, F., Atkin-Smith, G.K., et al. (2018). Minimal information for studies of extracellular vesicles 2018 (MISEV2018): a position statement of the International Society for Extracellular Vesicles and update of the MISEV2014 guidelines. Journal of Extracellular Vesicles *7*, 1535750. 10.1080/20013078.2018.1535750.

24. Zaborowski, M.P., Balaj, L., Breakefield, X.O., and Lai, C.P. (2015). Extracellular Vesicles: Composition, Biological Relevance, and Methods of Study. BioScience *65*, 783-797. 10.1093/biosci/biv084.

25. Zabeo, D., Cvjetkovic, A., Lässer, C., Schorb, M., Lötvall, J., and Höög, J.L. (2017). Exosomes purified from a single cell type have diverse morphology. J Extracell Vesicles *6*, 1329476. 10.1080/20013078.2017.1329476.

26. Trajkovic, K., Hsu, C., Chiantia, S., Rajendran, L., Wenzel, D., Wieland, F., Schwille, P., Brügger, B., and Simons, M. (2008). Ceramide triggers budding of exosome vesicles into multivesicular endosomes. Science *319*, 1244-1247. 10.1126/science.1153124.

27. Menck, K., Sönmezer, C., Worst, T.S., Schulz, M., Dihazi, G.H., Streit, F., Erdmann, G., Kling, S., Boutros, M., Binder, C., and Gross, J.C. (2017). Neutral sphingomyelinases control extracellular vesicles budding from the plasma membrane. J Extracell Vesicles *6*, 1378056. 10.1080/20013078.2017.1378056.

28. Fredman, G., Li, Y., Dalli, J., Chiang, N., and Serhan, C.N. (2012). Self-limited versus delayed resolution of acute inflammation: temporal regulation of pro-resolving mediators and microRNA. Sci Rep *2*, 639. 10.1038/srep00639.

29. Lemke, G., and Rothlin, C.V. (2008). Immunobiology of the TAM receptors. Nat Rev Immunol *8*, 327-336. 10.1038/nri2303.

30. Mehrotra, P., and Ravichandran, K.S. (2022). Drugging the efferocytosis process: concepts and opportunities. Nat Rev Drug Discov *21*, 601-620. 10.1038/s41573-022-00470-y.

31. Casella, J.F., Flanagan, M.D., and Lin, S. (1981). Cytochalasin D inhibits actin polymerization and induces depolymerization of actin filaments formed during platelet shape change. Nature *293*, 302-305. 10.1038/293302a0.

32. Wang, Y., Subramanian, M., Yurdagul, A., Jr., Barbosa-Lorenzi, V.C., Cai, B., de Juan-Sanz, J., Ryan, T.A., Nomura, M., Maxfield, F.R., and Tabas, I.

(2017). Mitochondrial Fission Promotes the Continued Clearance of Apoptotic Cells by Macrophages. Cell *171*, 331-345.e322. 10.1016/j.cell.2017.08.041.

33. Yeung, M.Y., McGrath, M.M., Nakayama, M., Shimizu, T., Boenisch, O., Magee, C.N., Abdoli, R., Akiba, H., Ueno, T., Turka, L.A., and Najafian, N. (2013). Interruption of dendritic cell-mediated TIM-4 signaling induces regulatory T cells and promotes skin allograft survival. J Immunol *191*, 4447-4455. 10.4049/jimmunol.1300992.

34. Meyer, R.C., Giddens, M.M., Coleman, B.M., and Hall, R.A. (2014). The protective role of prosaposin and its receptors in the nervous system. Brain Res *1585*, 1-12. 10.1016/j.brainres.2014.08.022.

35. Meyer, R.C., Giddens, M.M., Schaefer, S.A., and Hall, R.A. (2013). GPR37 and GPR37L1 are receptors for the neuroprotective and glioprotective factors prosaptide and prosaposin. Proc Natl Acad Sci U S A *110*, 9529-9534. 10.1073/pnas.1219004110.

36. Bang, S., Xie, Y.K., Zhang, Z.J., Wang, Z., Xu, Z.Z., and Ji, R.R. (2018). GPR37 regulates macrophage phagocytosis and resolution of inflammatory pain. J Clin Invest *128*, 3568-3582. 10.1172/jci99888.

37. Bang, S., Donnelly, C.R., Luo, X., Toro-Moreno, M., Tao, X., Wang, Z., Chandra, S., Bortsov, A.V., Derbyshire, E.R., and Ji, R.R. (2021). Activation of GPR37 in macrophages confers protection against infection-induced sepsis and pain-like behaviour in mice. Nat Commun *12*, 1704. 10.1038/s41467-021-21940-8.

38. Saadi, H., Shan, Y., Marazziti, D., and Wray, S. (2019). GPR37 Signaling Modulates Migration of Olfactory Ensheathing Cells and Gonadotropin Releasing Hormone Cells in Mice. Front Cell Neurosci *13*, 200. 10.3389/fncel.2019.00200.

39. Monje, P., Hernández-Losa, J., Lyons, R.J., Castellone, M.D., and Gutkind, J.S. (2005). Regulation of the transcriptional activity of c-Fos by ERK. A novel role for the prolyl isomerase PIN1. J Biol Chem *280*, 35081-35084. 10.1074/jbc.C500353200.

40. Stelzer, G., Rosen, N., Plaschkes, I., Zimmerman, S., Twik, M., Fishilevich, S., Stein, T.I., Nudel, R., Lieder, I., Mazor, Y., et al. (2016). The GeneCards Suite: From Gene Data Mining to Disease Genome Sequence Analyses. Current Protocols in Bioinformatics *54*, 1.30.31-31.30.33. https://doi.org/10.1002/cpbi.5.

41. Fanjul, A., Dawson, M.I., Hobbs, P.D., Jong, L., Cameron, J.F., Harlev, E., Graupner, G., Lu, X.-P., and Pfahl, M. (1994). A new class of retinoids with selective inhibition of AP-1 inhibits proliferation. Nature *372*, 107-111. 10.1038/372107a0.

42. van Leent, M.M.T., Beldman, T.J., Toner, Y.C., Lameijer, M.A., Rother, N., Bekkering, S., Teunissen, A.J.P., Zhou, X., van der Meel, R., Malkus, J., et al.

(2021). Prosaposin mediates inflammation in atherosclerosis. Sci Transl Med *13*. 10.1126/scitranslmed.abe1433.

43. Park, D., Han, C.Z., Elliott, M.R., Kinchen, J.M., Trampont, P.C., Das, S., Collins, S., Lysiak, J.J., Hoehn, K.L., and Ravichandran, K.S. (2011). Continued clearance of apoptotic cells critically depends on the phagocyte Ucp2 protein. Nature *477*, 220-224. 10.1038/nature10340.

44. Yurdagul, A., Subramanian, M., Wang, X., Crown, S.B., Ilkayeva, O.R., Darville, L., Kolluru, G.K., Rymond, C.C., Gerlach, B.D., Zheng, Z., et al. (2020). Macrophage Metabolism of Apoptotic Cell-Derived Arginine Promotes Continual Efferocytosis and Resolution of Injury. Cell Metabolism *31*, 518-533.e510. https://doi.org/10.1016/j.cmet.2020.01.001.

45. Ampomah, P.B., Cai, B., Sukka, S.R., Gerlach, B.D., Yurdagul, A., Jr., Wang, X., Kuriakose, G., Darville, L.N.F., Sun, Y., Sidoli, S., et al. (2022). Macrophages use apoptotic cell-derived methionine and DNMT3A during efferocytosis to promote tissue resolution. Nat Metab *4*, 444-457. 10.1038/s42255-022-00551-7.

46. Morioka, S., Perry, J.S.A., Raymond, M.H., Medina, C.B., Zhu, Y., Zhao, L., Serbulea, V., Onengut-Gumuscu, S., Leitinger, N., Kucenas, S., et al. (2018). Efferocytosis induces a novel SLC program to promote glucose uptake and lactate release. Nature *563*, 714-718. 10.1038/s41586-018-0735-5.

47. Gerlach, B.D., Ampomah, P.B., Yurdagul, A., Jr., Liu, C., Lauring, M.C., Wang, X., Kasikara, C., Kong, N., Shi, J., Tao, W., and Tabas, I. (2021). Efferocytosis induces macrophage proliferation to help resolve tissue injury. Cell Metab *33*, 2445-2463.e2448. 10.1016/j.cmet.2021.10.015.

48. Kobayashi, N., Karisola, P., Peña-Cruz, V., Dorfman, D.M., Jinushi, M., Umetsu, S.E., Butte, M.J., Nagumo, H., Chernova, I., Zhu, B., et al. (2007). TIM-1 and TIM-4 glycoproteins bind phosphatidylserine and mediate uptake of apoptotic cells. Immunity *27*, 927-940. 10.1016/j.immuni.2007.11.011.

49. Flannagan, R.S., Canton, J., Furuya, W., Glogauer, M., and Grinstein, S. (2014). The phosphatidylserine receptor TIM4 utilizes integrins as coreceptors to effect phagocytosis. Mol Biol Cell *25*, 1511-1522. 10.1091/mbc.E13-04-0212.

50. Moon, B., Lee, J., Lee, S.A., Min, C., Moon, H., Kim, D., Yang, S., Moon, H., Jeon, J., Joo, Y.E., and Park, D. (2020). Mertk Interacts with Tim-4 to Enhance Tim-4-Mediated Efferocytosis. Cells *9*. 10.3390/cells9071625.

51. Thorp, E., Vaisar, T., Subramanian, M., Mautner, L., Blobel, C., and Tabas, I. (2011). Shedding of the Mer tyrosine kinase receptor is mediated by ADAM17 protein through a pathway involving reactive oxygen species, protein kinase Cδ, and p38 mitogen-activated protein kinase (MAPK). J Biol Chem *286*, 33335-33344. 10.1074/jbc.M111.263020.

52. Bouchareychas, L., Duong, P., Phu, T.A., Alsop, E., Meechoovet, B., Reiman, R., Ng, M., Yamamoto, R., Nakauchi, H., Gasper, W.J., et al. (2021). High glucose macrophage exosomes enhance atherosclerosis by driving cellular proliferation & hematopoiesis. iScience *24*, 102847. 10.1016/j.isci.2021.102847.

53. Zhang, Y.G., Song, Y., Guo, X.L., Miao, R.Y., Fu, Y.Q., Miao, C.F., and Zhang, C. (2019). Exosomes derived from oxLDL-stimulated macrophages induce neutrophil extracellular traps to drive atherosclerosis. Cell Cycle *18*, 2674-2684. 10.1080/15384101.2019.1654797.

54. Bouchareychas, L., Duong, P., Covarrubias, S., Alsop, E., Phu, T.A., Chung, A., Gomes, M., Wong, D., Meechoovet, B., Capili, A., et al. (2020). Macrophage Exosomes Resolve Atherosclerosis by Regulating Hematopoiesis and Inflammation via MicroRNA Cargo. Cell Reports *32*, 107881. https://doi.org/10.1016/j.celrep.2020.107881.

55. Patil, M., Saheera, S., Dubey, P.K., Kahn-Krell, A., Govindappa, P.K., Singh, S., Tousif, S., Zhang, Q., Lal, H., Zhang, J., et al. (2021). Novel Mechanisms of Exosome-Mediated Phagocytosis of Dead Cells in Injured Heart. Circulation Research *129*, 1006-1020. doi:10.1161/CIRCRESAHA.120.317900.

56. de Couto, G., Jaghatspanyan, E., DeBerge, M., Liu, W., Luther, K., Wang, Y., Tang, J., Thorp, E.B., and Marbán, E. (2019). Mechanism of Enhanced MerTK-Dependent Macrophage Efferocytosis by Extracellular Vesicles. Arterioscler Thromb Vasc Biol *39*, 2082-2096. 10.1161/atvbaha.119.313115.

57. O'Brien, J.S., and Kishimoto, Y. (1991). Saposin proteins: structure, function, and role in human lysosomal storage disorders. Faseb j *5*, 301-308. 10.1096/fasebj.5.3.2001789.

58. N V Lakshmi Kavya, A., Subramanian, S., and Ramakrishna, S. (2022). Therapeutic applications of exosomes in various diseases: A review. Biomaterials Advances *134*, 112579. https://doi.org/10.1016/j.msec.2021.112579.

59. Rezaie, J., Feghhi, M., and Etemadi, T. (2022). A review on exosomes application in clinical trials: perspective, questions, and challenges. Cell Communication and Signaling *20*, 145. 10.1186/s12964-022-00959-4.

60. Khan, A.I., Kapoor, A., Chen, J., Martin, L., Rogazzo, M., Mercier, T., Decosterd, L., Collino, M., and Thiemermann, C. (2018). The Antimalarial Drug Artesunate Attenuates Cardiac Injury in A Rodent Model of Myocardial Infarction. Shock *49*, 675-681. 10.1097/shk.0000000000000963.

61. Zhang, X., Goncalves, R., and Mosser, D.M. (2008). The isolation and characterization of murine macrophages. Curr Protoc Immunol *Chapter 14*, 14.11.11-14.11.14. 10.1002/0471142735.im1401s83.

62. Théry, C., Amigorena, S., Raposo, G., and Clayton, A. (2006). Isolation and Characterization of Exosomes from Cell Culture Supernatants and Biological Fluids. Current Protocols in Cell Biology *30*, 3.22.21-23.22.29. https://doi.org/10.1002/0471143030.cb0322s30.

63. Dhawan, U.K., Bhattacharya, P., Narayanan, S., Manickam, V., Aggarwal, A., and Subramanian, M. (2021). Hypercholesterolemia Impairs Clearance of Neutrophil Extracellular Traps and Promotes Inflammation and Atherosclerotic Plaque Progression. Arteriosclerosis, Thrombosis, and Vascular Biology *41*, 2598-2615. doi:10.1161/ATVBAHA.120.316389.

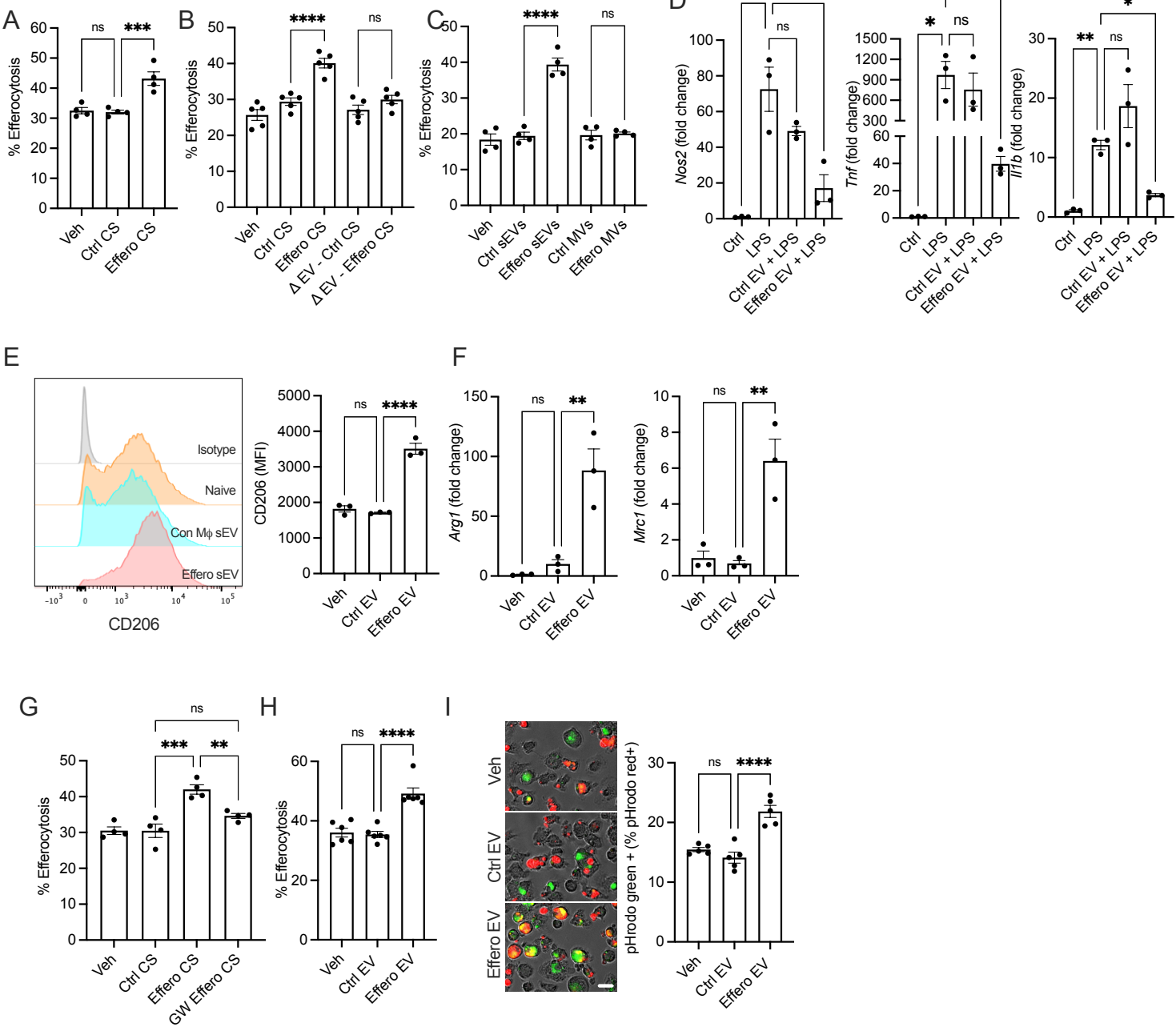
A
% Efferocytosis
ns
***
Veh
Ctrl CS
Effero CS
B
% Efferocytosis
****
ns
Veh
Ctrl CS
Effero CS
Δ EV - Ctrl CS
Δ EV - Effero CS
C
% Efferocytosis
****
ns
Veh
Ctrl sEVs
Effero sEVs
Ctrl MVs
Effero MVs
D
Nos2 (fold change)
***
**
ns
Tnf (fold change)
*
*
ns
Il1b (fold change)
**
*
ns
Ctrl
LPS
Ctrl EV + LPS
Effero EV + LPS
E
Isotype
Naive
Con Mϕ sEV
Effero sEV
CD206
CD206 (MFI)
ns
****
Veh
Ctrl EV
Effero EV
F
Arg1 (fold change)
ns
**
Mrc1 (fold change)
ns
**
Veh
Ctrl EV
Effero EV
G
% Efferocytosis
ns
***
**
Veh
Ctrl CS
Effero CS
GW Effero CS
H
% Efferocytosis
ns
****
Veh
Ctrl EV
Effero EV
I
Veh
Ctrl EV
Effero EV
pHrodo green + (% pHrodo red+)
ns
****
Veh
Ctrl EV
Effero EV

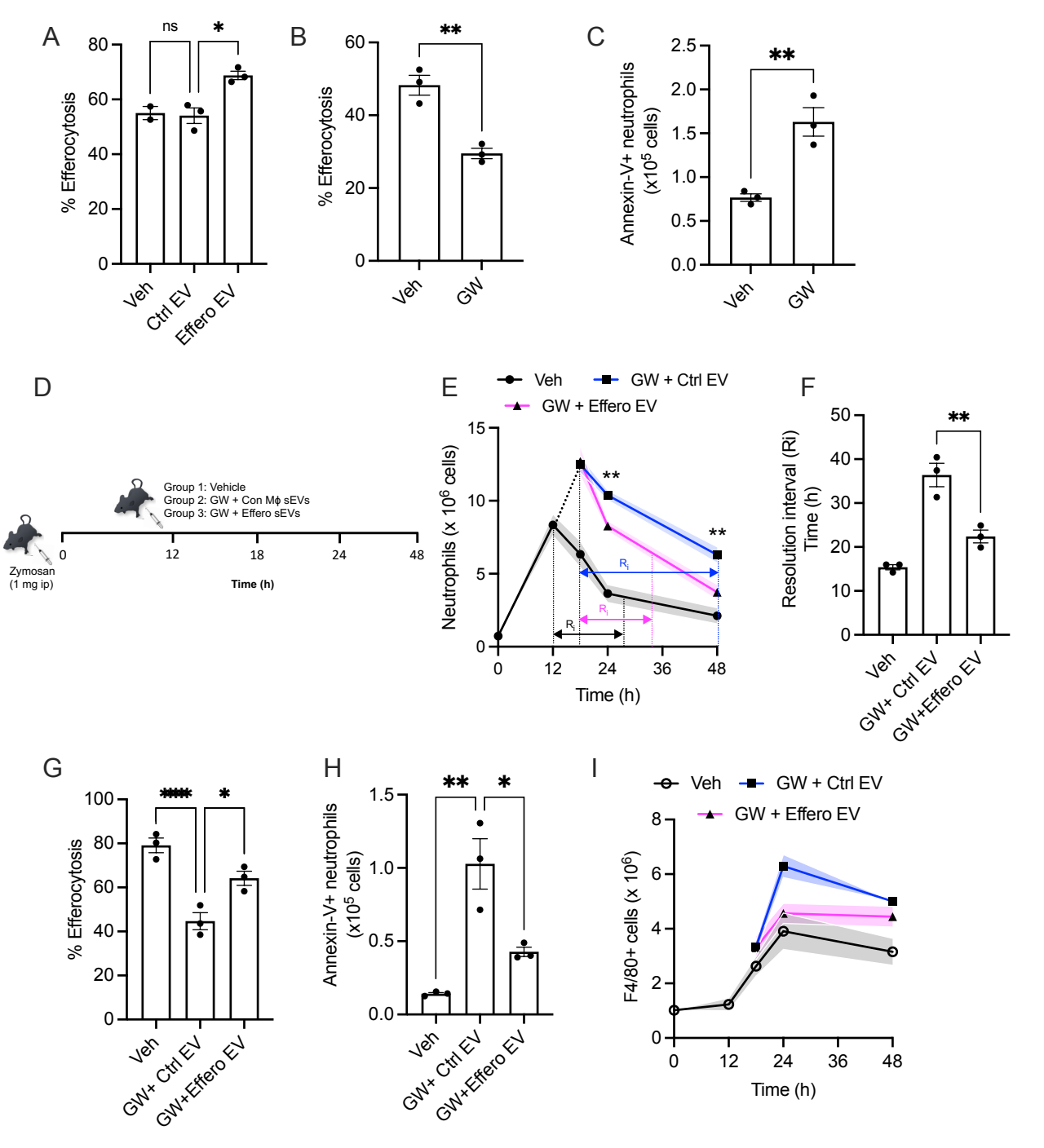
A
ns
*
% Efferocytosis
Veh
Ctrl EV
Effero EV
B
**
% Efferocytosis
Veh
GW
C
**
Annexin-V+ neutrophils (x10^5 cells)
Veh
GW
D
Group 1: Vehicle
Group 2: GW + Con Mϕ sEVs
Group 3: GW + Effero sEVs
Zymosan (1 mg ip)
Time (h)
E
Veh
GW + Ctrl EV
GW + Effero EV
Neutrophils (x 10^6 cells)
Time (h)
F
**
Resolution interval (Ri) Time (h)
Veh
GW+ Ctrl EV
GW+Effero EV
G
****
*
% Efferocytosis
Veh
GW+ Ctrl EV
GW+Effero EV
H
**
*
Annexin-V+ neutrophils (x10^5 cells)
Veh
GW+ Ctrl EV
GW+Effero EV
I
Veh
GW + Ctrl EV
GW + Effero EV
F4/80+ cells (x 10^6)
Time (h)

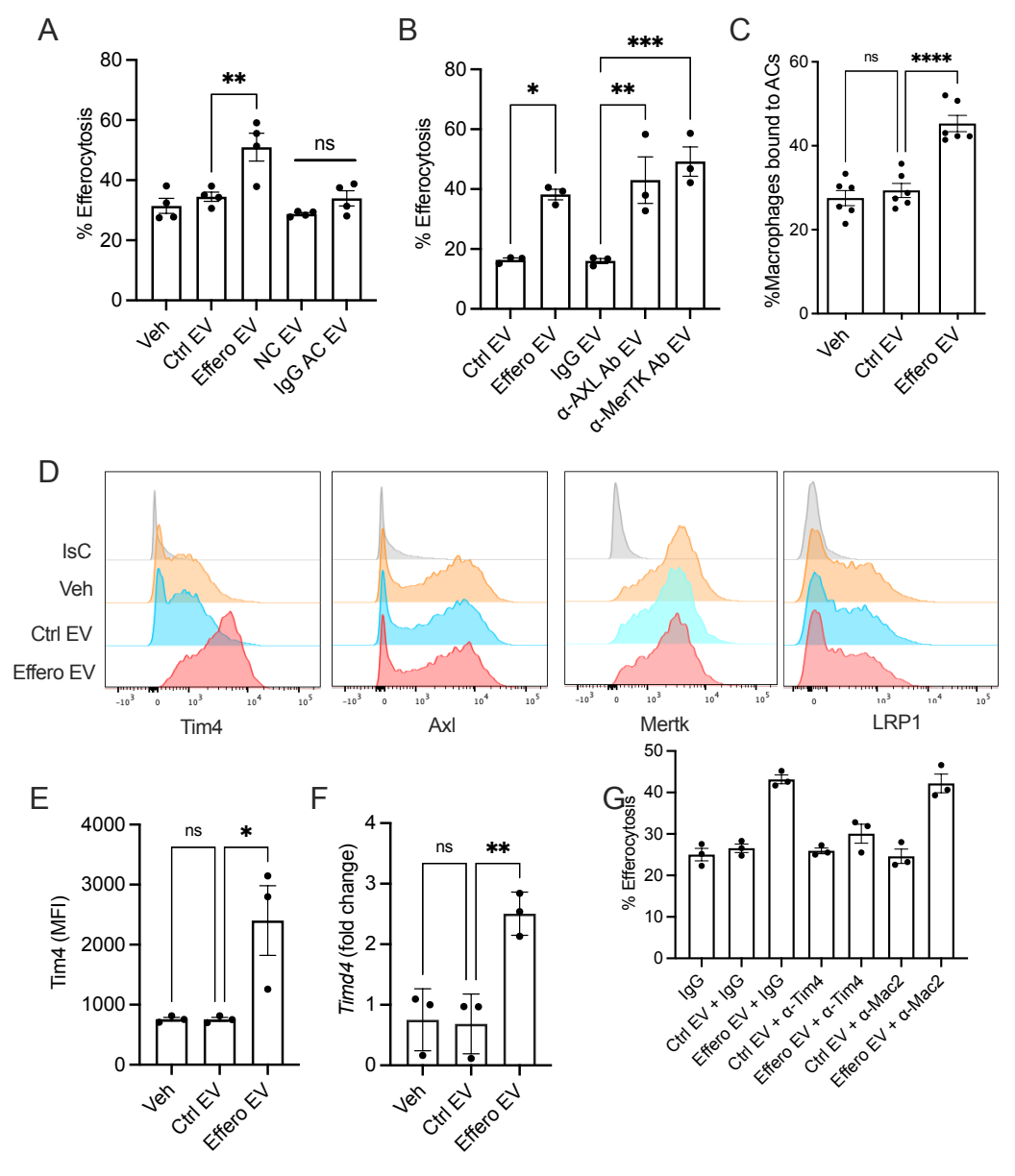
A
% Efferocytosis
Veh
Ctrl EV
Effero EV
NC EV
IgG AC EV
B
% Efferocytosis
Ctrl EV
Effero EV
IgG EV
α-AXL Ab EV
α-MerTK Ab EV
C
%Macrophages bound to ACs
Veh
Ctrl EV
Effero EV
D
IsC
Veh
Ctrl EV
Effero EV
Tim4
Axl
Mertk
LRP1
E
Tim4 (MFI)
Veh
Ctrl EV
Effero EV
F
Timd4 (fold change)
Veh
Ctrl EV
Effero EV
G
% Efferocytosis
IgG
Ctrl EV + IgG
Effero EV + IgG
Ctrl EV + α-Tim4
Effero EV + α-Tim4
Ctrl EV + α-Mac2
Effero EV + α-Mac2

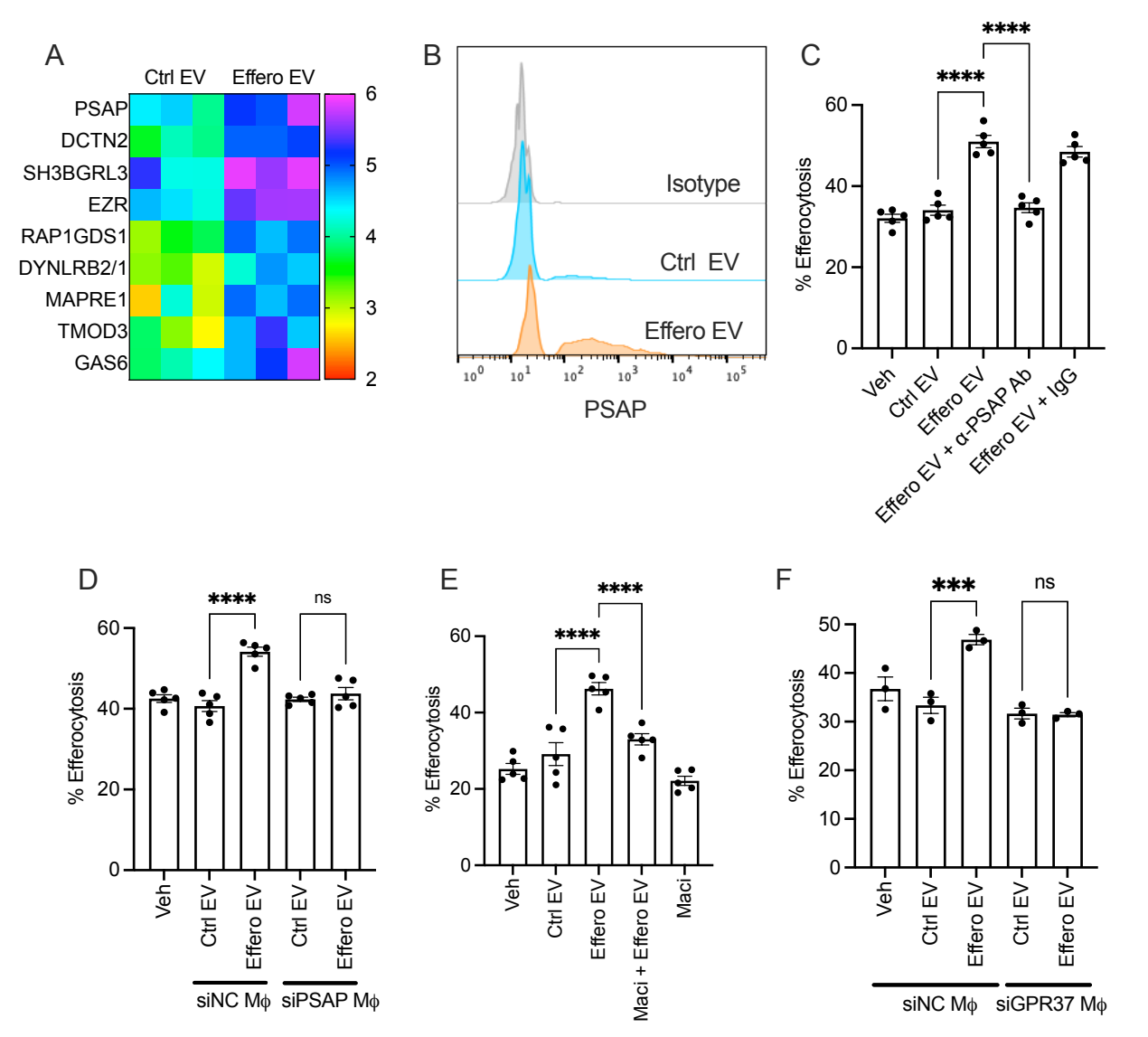
A
Ctrl EV
Effero EV
PSAP
DCTN2
SH3BGRL3
EZR
RAP1GDS1
DYNLRB2/1
MAPRE1
TMOD3
GAS6
6
5
4
3
2
B
Isotype
Ctrl EV
Effero EV
PSAP
C
% Efferocytosis
Veh
Ctrl EV
Effero EV
Effero EV + α-PSAP Ab
Effero EV + IgG
D
% Efferocytosis
ns
Veh
Ctrl EV
Effero EV
siNC Mϕ
siPSAP Mϕ
E
% Efferocytosis
Veh
Ctrl EV
Effero EV
Maci + Effero EV
Maci
F
% Efferocytosis
ns
siNC Mϕ
siGPR37 Mϕ

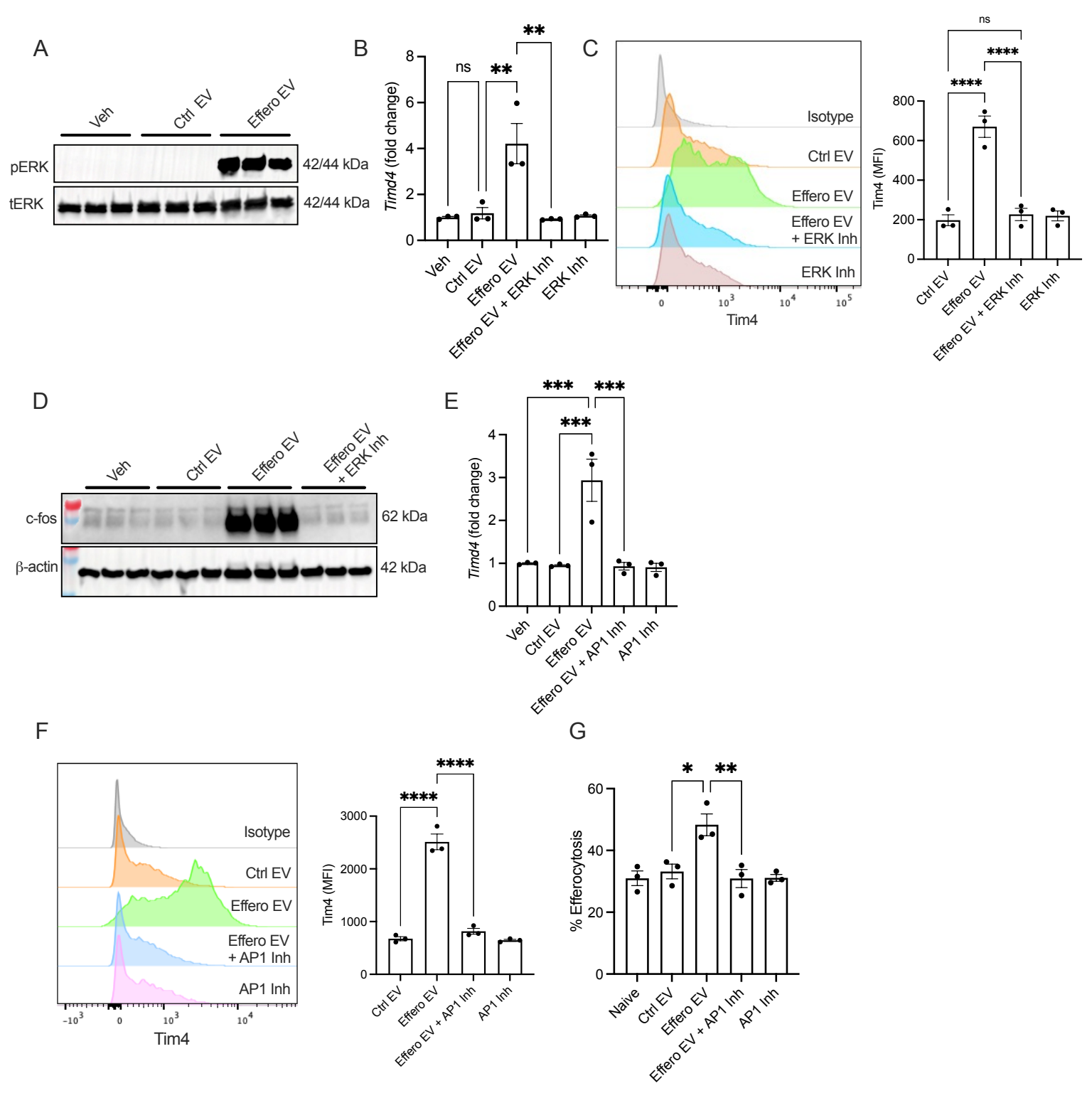
A
Veh
Ctrl EV
Effero EV
pERK
tERK
42/44 kDa
42/44 kDa
B
Timd4 (fold change)
ns
**
**
Veh
Ctrl EV
Effero EV
Effero EV + ERK Inh
ERK Inh
C
Isotype
Ctrl EV
Effero EV
Effero EV + ERK Inh
ERK Inh
Tim4
ns
****
****
Tim4 (MFI)
Ctrl EV
Effero EV
Effero EV + ERK Inh
ERK Inh
D
Veh
Ctrl EV
Effero EV
Effero EV + ERK Inh
c-fos
β-actin
62 kDa
42 kDa
E
Timd4 (fold change)
***
***
***
Veh
Ctrl EV
Effero EV
Effero EV + AP1 Inh
AP1 Inh
F
Isotype
Ctrl EV
Effero EV
Effero EV + AP1 Inh
AP1 Inh
Tim4
****
****
Tim4 (MFI)
Ctrl EV
Effero EV
Effero EV + AP1 Inh
AP1 Inh
G
*
**
% Efferocytosis
Naive
Ctrl EV
Effero EV
Effero EV + AP1 Inh
AP1 Inh

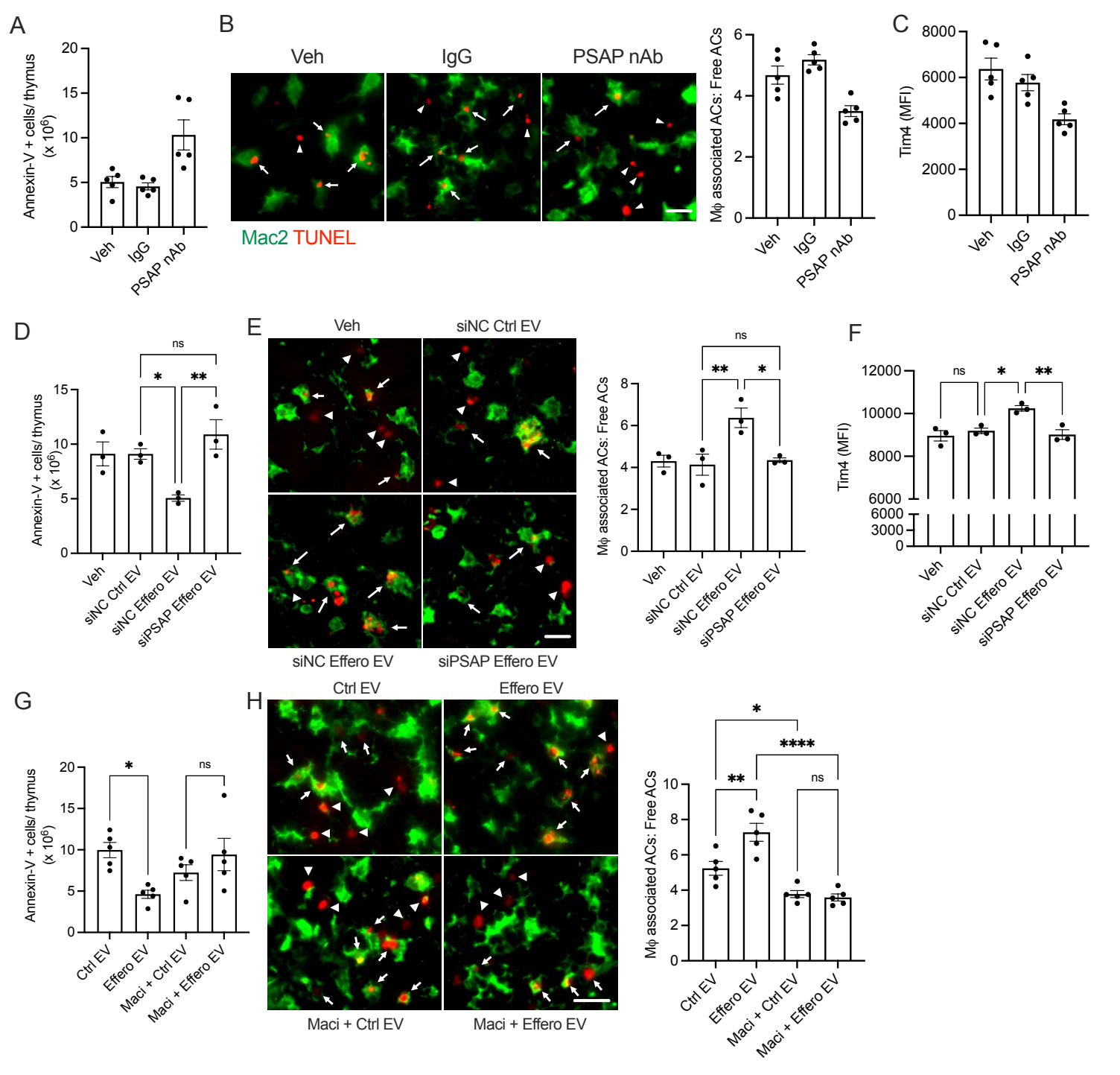
A
Annexin-V + cells/ thymus (x 10^6)
Veh
IgG
PSAP nAb
B
Veh
IgG
PSAP nAb
Mac2 TUNEL
Mϕ associated ACs: Free ACs
C
Tim4 (MFI)
D
ns
*
**
siNC Ctrl EV
siNC Effero EV
siPSAP Effero EV
E
Veh
siNC Ctrl EV
siNC Effero EV
siPSAP Effero EV
F
G
Ctrl EV
Effero EV
Maci + Ctrl EV
Maci + Effero EV
H
****

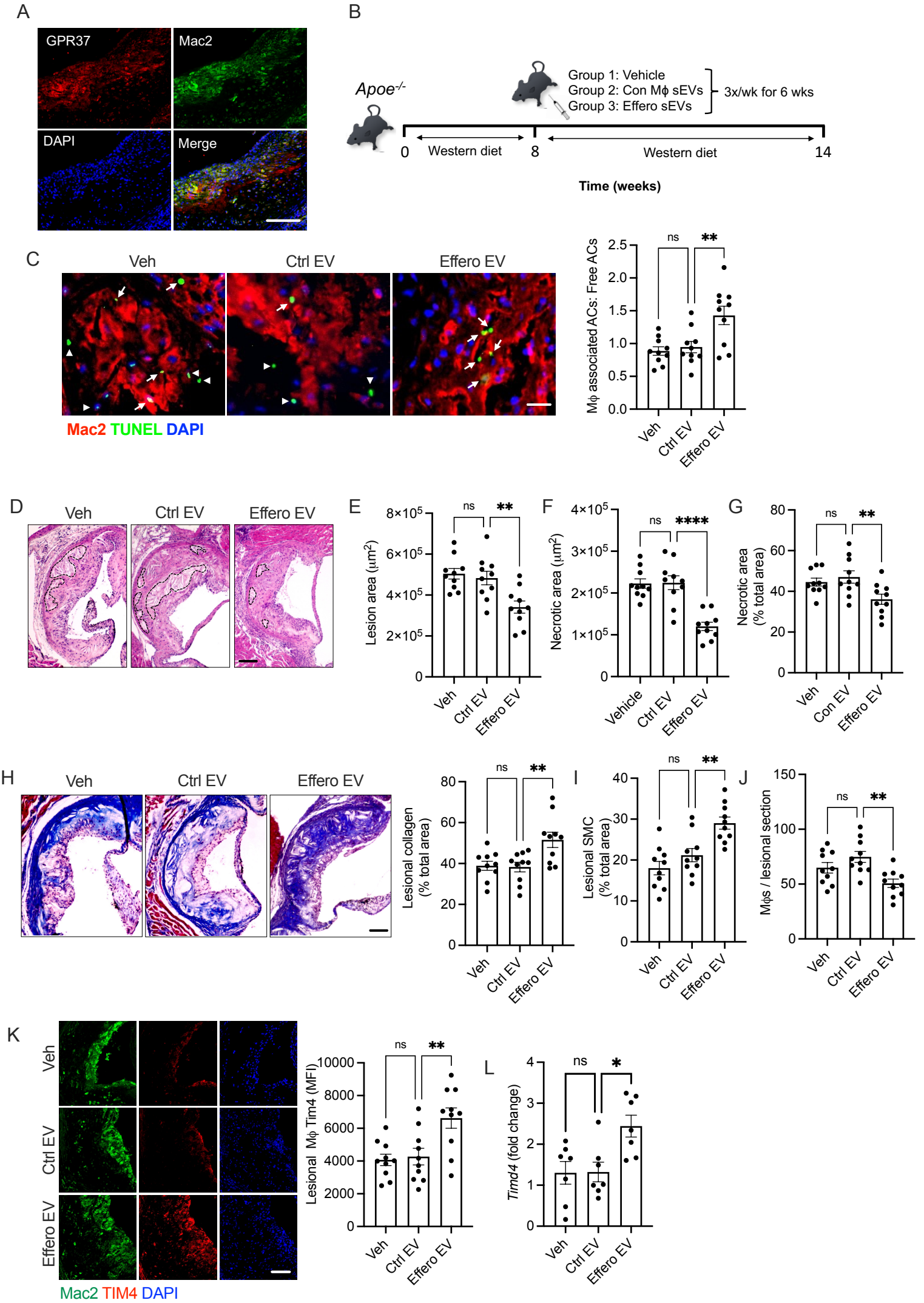
A
GPR37
Mac2
DAPI
Merge
B
Apoe-/-
Group 1: Vehicle
Group 2: Con Mϕ sEVs
Group 3: Effero sEVs
3x/wk for 6 wks
0
Western diet
8
Western diet
14
Time (weeks)
C
Veh
Ctrl EV
Effero EV
Mac2 TUNEL DAPI
Mϕ associated ACs: Free ACs
ns
**
Veh
Ctrl EV
Effero EV
D
Veh
Ctrl EV
Effero EV
E
Lesion area (μm2)
ns
**
Veh
Ctrl EV
Effero EV
F
Necrotic area (μm2)
ns
****
Vehicle
Ctrl EV
Effero EV
G
Necrotic area (% total area)
ns
**
Veh
Con EV
Effero EV
H
Veh
Ctrl EV
Effero EV
Lesional collagen (% total area)
ns
**
Veh
Ctrl EV
Effero EV
I
Lesional SMC (% total area)
ns
**
Veh
Ctrl EV
Effero EV
J
Mϕs / lesional section
ns
**
Veh
Ctrl EV
Effero EV
K
Veh
Ctrl EV
Effero EV
Mac2 TIM4 DAPI
Lesional Mϕ Tim4 (MFI)
ns
**
Veh
Ctrl EV
Effero EV
L
Timd4 (fold change)
ns
*
Veh
Ctrl EV
Effero EV

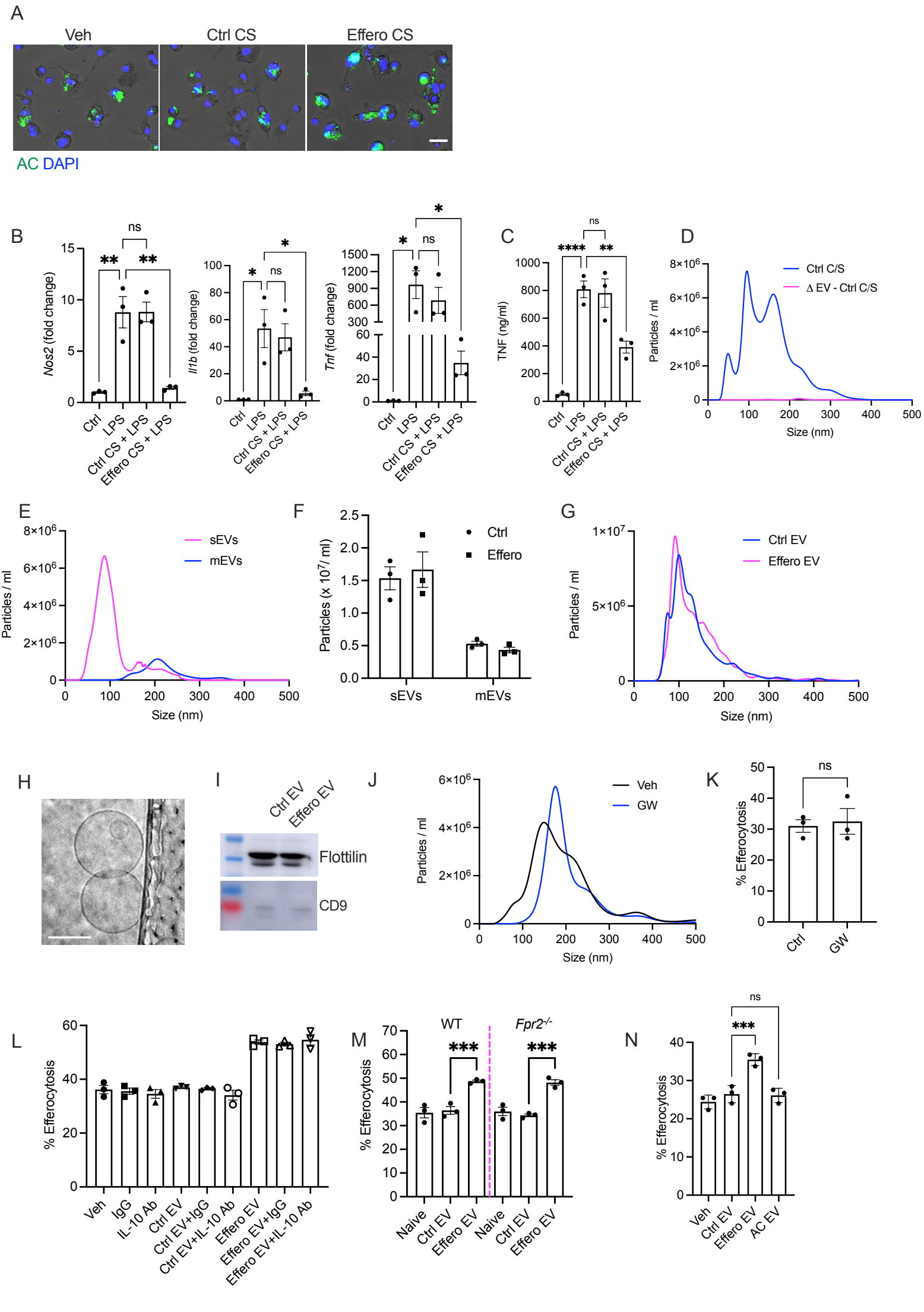
A
Veh
Ctrl CS
Effero CS
AC DAPI
B
Nos2 (fold change)
Il1b (fold change)
Tnf (fold change)
Ctrl
LPS
Ctrl CS + LPS
Effero CS + LPS
ns
C
TNF (ng/ml)
D
Particles / ml
Ctrl C/S
Δ EV - Ctrl C/S
Size (nm)
E
sEVs
mEVs
F
Particles (x 10^7/ ml)
Ctrl
Effero
G
Ctrl EV
Effero EV
H
I
Flottilin
CD9
J
Veh
GW
K
% Efferocytosis
L
Veh
IgG
IL-10 Ab
Ctrl EV
Ctrl EV+IgG
Ctrl EV+IL-10 Ab
Effero EV
Effero EV+IgG
Effero EV+IL-10 Ab
M
WT
Fpr2-/-
Naive
N
AC EV

Figure S1. Physical and functional characterisation of Effero-EVs (A) BMDMs were incubated with supernatants derived from Ctrls (Ctrl CS) or efferocytes (Effero CS) for 16 h followed by incubation with fluorescently labelled ACs (green) for 1 h. After washing away unengulfed ACs, images were captured using a fluorescence microscope. **(B)** qPCR-based analysis for quantification of expression levels of *Nos2*, *Il1b*, and *Tnf* in cDNA isolated from BMDMs incubated with supernatants derived from control Mϕs (Ctrl CS) or efferocytes (Effero CS) followed by exposure to LPS (10 ng/mL) for 6 h. **(C)** The culture supernatant from the above experiment was used for quantification of secreted levels of TNF by ELISA. **(D-F)** Representative nanoparticle tracker analyzer (NTA) histogram showing **(D)** particle distribution in Ctrl CS and EV-depleted Ctrl CS, **(E)** purity of EVs and MVs isolated by differential ultracentrifugation from Ctrl CS, **(F)** particle concentration of EVs and mEVs, and **(G)** size distribution of EVs isolated from Ctrl and efferocytes. **(H)** Representative cryo-EM image of EVs isolated from efferocytes. Bar, 100 nm. **(I)** Immunoblotting for flotillin and CD9 in lysates obtained from control EVs and Effero EVs. **(J)** NTA histogram showing concentration and size distribution of particles in culture supernatants of Mϕs treated with vehicle or GW4869 (5 μM). **(K)** Analysis of efferocytosis efficiency of BMDMs treated with vehicle or GW4869. **(L)** Efferocytosis assay in BMDMs incubated with Ctrl EVs or Effero-EVs in the presence of an IL-10 neutralizing antibody or appropriate isotype control antibody. **(M)** Quantification of efferocytosis efficiency of WT and FPR2 KO BMDMs incubated with Ctrl EVs or Effero-EVs. **(N)** BMDMs were incubated with EVs isolated from supernatants of cultured ACs or control Mϕ or efferocytes followed by quantification of efferocytosis efficiency.

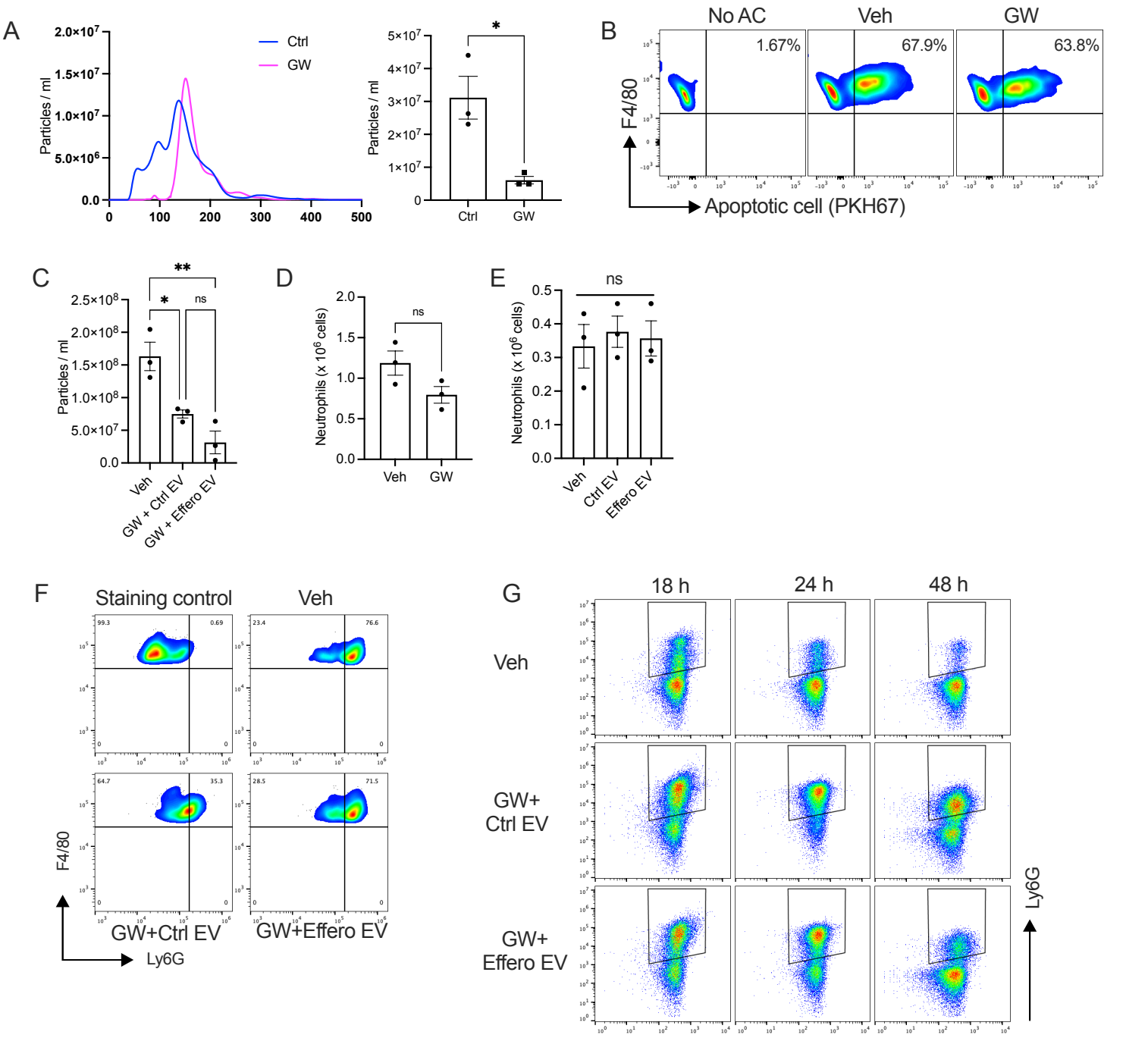

Figure S2. Effero-EVs resolve inflammation *in vivo*. (A) C57BL/6 mice were injected vehicle or GW4869 (2 mg/kg) intraperitoneally followed by lavage 12 h post-injection. The lavage fluid was subjected to NTA to analyze the size distribution of particles (left panel) and the concentration of vesicles < 120 nm size (right panel). (B) Vehicle or GW4869-administered mice were injected with 1x10^6 PKH67-labelled ACs intraperitoneally. 45 min post-injection, peritoneal lavage was conducted, and the cells were immunostained with anti-F4/80 antibody followed by flow cytometry. Efferocytosis was calculated as the percent F4/80+ cells that co-express PKH67 signal. (C) C57BL/6 mice were injected zymosan (1 mg) intraperitoneally. 12 h later, the mice were administered GW4869 (2 mg/kg) along with Ctrl EVs or Effero EVs. Peritoneal lavage was collected 6 h post-injection of GW4869 and the concentration of EVs was quantified by NTA. (D) C57BL/6 mice were injected PBS (vehicle) or GW4869 intraperitoneally. 6 h post-injection, peritoneal lavage was performed, and cells were immunostained with anti-Ly6G antibody. Flow-cytometry was conducted to quantify the number of Ly6G+ neutrophils. (E) C57BL/6 mice were injected either vehicle, Ctrl EVs or Effero EVs and 12 h post-injection the peritoneal lavage was analyzed for the numbers of Ly6G+ neutrophils by flow cytometry. (F) 10-week old female C57BL/6 mice were injected 1mg zymosan intraperitoneally and 12 h later were randomized into 3 groups. One group received PBS (vehicle) while appropriate groups received GW4869 (2 mg/kg ip) along with either Ctrl EVs or Effero EVs (30 µg EV protein). Mice were euthanized at indicated time points and the 18 h peritoneal lavage was analyzed by flow cytometry to quantify the % F4/80+ Mϕs that co-express Ly6G intracellularly as an indicator of efferocytosis efficiency. Staining control represents cells non-permeabilized cells. (G) As above except that flow cytometry was conducted to analyze the numbers of Ly6G+ neutrophils.

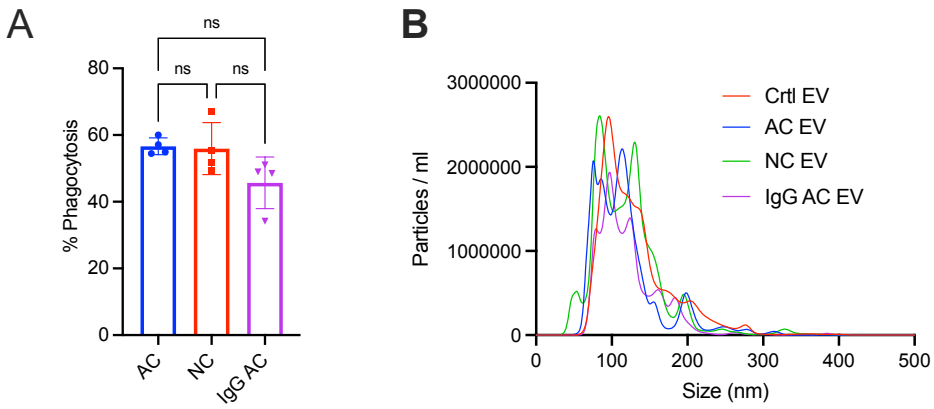

Figure S3. Mϕs engulf distinct phagocytic targets and release equivalent numbers of EVs. (A) BMDMs were incubated with fluorescently labelled ACs, necrotic cells, or IgG-opsonized ACs at a ratio of 1:5 for 2 h followed by fluorescence microscopy for quantification of phagocytic efficiency. **(B)** NTA for quantification of concentration of EVs isolated from supernatants of Mϕs that have engulfed either ACs (AC), necrotic cells (NC), or IgG-coated AC (IgG AC).

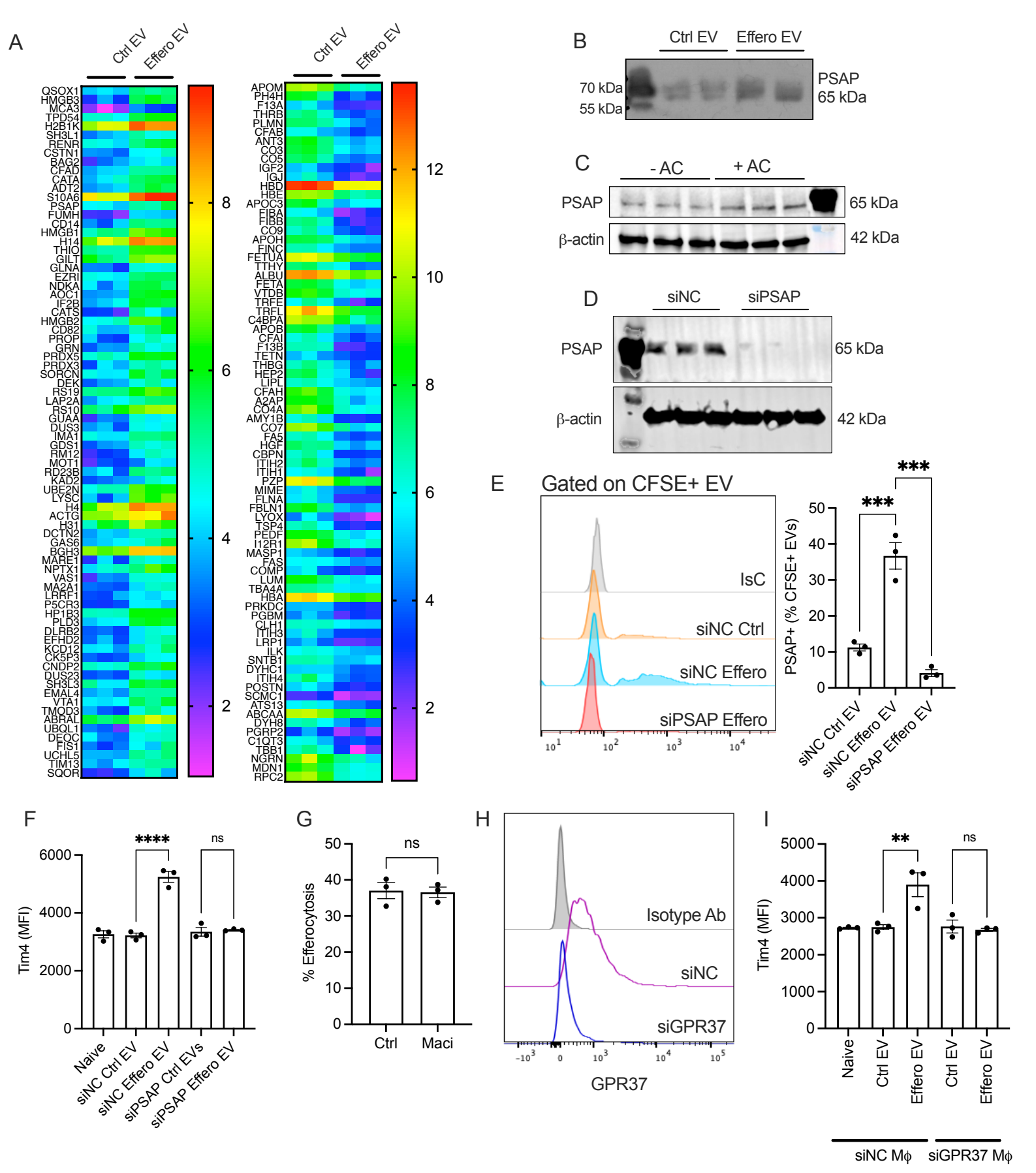

Figure S4. Proteomic analysis of Effero-EVs and functional validation of differentially expressed cargo. (A) Heatmap of proteins that were upregulated (left panel) or downregulated (right panel) in Effero EVs as compared with control EVs derived from THP-1 Mϕs. (B) Immunoblotting for analysis of PSAP expression in EV lysates obtained from Ctrls or efferocytes. (C) Immunoblotting analysis of PSAP expression in whole cell lysates of Ctrl Mϕs or efferocytes. (D) Analysis of PSAP expression in whole cell lysates obtained from BMDMs transfected with either negative control siRNA (siNC) or PSAP siRNA (siPSAP) (E) Effero EVs were isolated from Mφs transfected with negative control siRNA (siNC) or PSAP siRNA (siPSAP). Nano-flowcytometry was performed to analyze the expression levels of PSAP on EVs. (F) Analysis of Tim4 expression in BMDMs exposed to Effero EVs or PSAP-knockdown Effero EVs. (G) Efferocytosis assay in BMDMs treated with vehicle of macitentan (10 nM) for 16 h. (H) Flow cytometric analysis of cell surface expression of GPR37 in BMDMs transfected with either negative control siRNA (siNC) or GPR37 siRNA (siGPR37). (I) Flow-cytometric quantification of cell surface expression of Tim4 in WT (siNC Mϕ) or GPR37 knockdown Mφs (siGPR37 Mϕ) upon exposure to Ctrl EVs or Effero EVs.

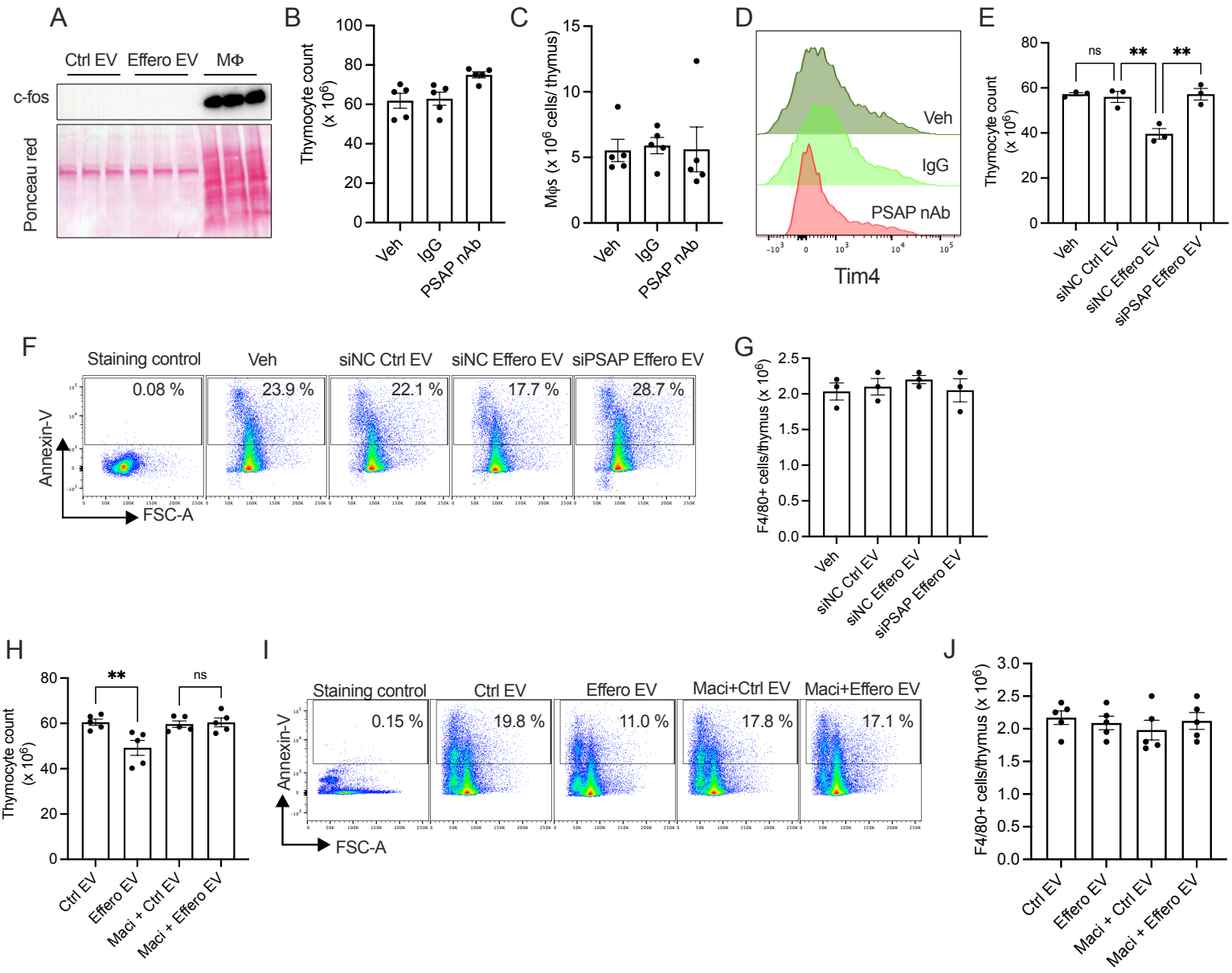

Figure S5. Functional validation of PSAP-GPR37 signalling in enhancing Mϕ efferocytosis *in vivo*. **(A)** Analysis of c-fos expression in efferocyte whole cell lysates or lysates obtained from Ctrl- and Effero-EVs. Analysis of **(B)** total thymocyte count, and **(C)** total numbers of thymic F4/80+ Mϕs, and **(D)** Tim4 expression levels in thymic Mϕs in mice injected with dexamethasone (250 µg/ mouse) intraperitoneally along with PBS (veh), anti-PSAP neutralising Ab (PSAP nAb), or IgG control. **(E-G)** Analysis of total thymocyte count, **(F)** numbers of annexin-V+ thymic cells, and **(G)** numbers of thymic Mϕs in mice administered dexamethasone followed by intravenous injection of Ctrl EVs or Effero EVs isolated from either PSAP knockdown (siPSAP) or Ctrls (siNC). **(H-J)** As above, except that mice were adminstered dexamethasone in the absence or presence of macitentan (maci). n = 5 mice per group.

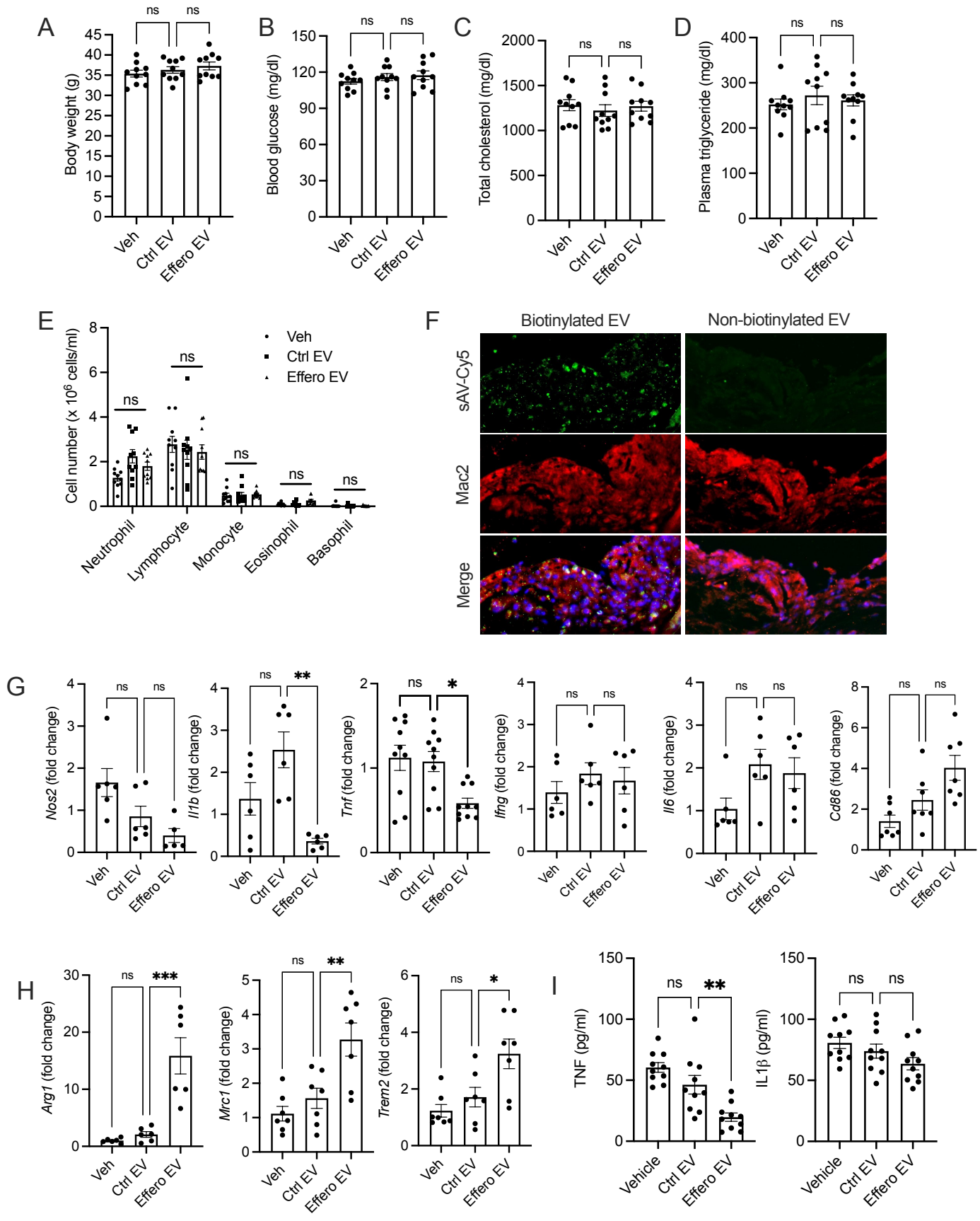

Figure S6. Analysis of atherosclerotic plaque progression in mice treated with Effero-EVs. Western diet-fed *Apoe*$^{-/-}$ mice were administered PBS (vehicle), Ctrl EVs, or Effero EVs and the following parameters were quantified: (A) Body weight, (B) 5 h fasting blood glucose, (C) plasma total cholesterol, (D) plasma triglyceride, and (E) differential leukocyte counts. (F) Aortic root sections of mice injected with biotinylated or non-biotinylated EVs were stained with streptavidin conjugated to Cy5 (sAV-Cy5, green) and anti-Mac2 antibody (red) and imaged using fluorescence microscopy. Nuclei were stained with DAPI (blue). (G and H) q-PCR-based analysis of expression of indicated genes in cDNA isolated from carotid arteries of appropriate groups of mice. (I) Analysis of plasma TNF and IL1β in indicated groups of *Apoe*$^{-/-}$ mice.